RADIATION EXPOSURE LEVELS ASSOCIATED WITH CONSTRUCTION SAND FROM THARAKA-NITHI COUNTY IN KENYA

KAMUNDE KARIMI BETTY

I56/CE/24516/2012

A Thesis Submitted in Partial Fulfillment of the Requirements for the Award of the Degree of Master of Science (Physics) in the School of Pure and Applied Sciences of Kenyatta University

MAY, 2016

DECLARATION

This thesis is my original work and has not been presented for a degree in any other university or any other award.

Signature ..... Date 06/05/2016

Karimi Kamunde (I56/CE/24516/2012)

Department of Physics

SUPERVISORS

We confirm that work reported in this thesis was carried out by the candidate under our supervision.

Signature ..... Date 06/05/2016

DR. Nadir Hashim

Department of Physics

Kenyatta University

Signature ..... Date 6/5/2016

DR. Sarroney Merenga

Department of Physics

Kenyatta University

DEDICATION

This thesis is dedicated to my son Jayden Baraka for his patience and encouragement, my dad Simon Kamunde, my late mum Agnes Kanyua and my mum Lucy Kagendo.

ACKNOWLEDGEMENTS

My greatest commendation goes to my research supervisors, Dr. Nadir Hashim and Dr. Sarroney Merenga for their whole hearted and valuable suggestions, advice, encouragement and supervision. Without them, this study would not have been such a success. I also thank the whole Kenyatta University Physics Department for providing laboratory facilities, technical staff and internet services for accessing scientific journals. Special thanks go to all the laboratory technicians for their support during this work.

This work could not have gone this far without the utmost support of my sister Elsie and her husband Peter. They took proper care of my son and gave me moral and financial support throughout my study period without feeling burdened. They made my studies a great success and I will forever be indebted. I also want to appreciate my son Jayden Baraka, for the immense encouragement and understanding he accorded me during this work. He was such a motivator that has propelled me this far. Sincere gratitude goes to all my family for their immeasurable support during this period. My heart felt gratitude goes to my employer TSC for giving me a study leave to conduct my research, that time meant a lot to my studies.

Above all am sincerely grateful to almighty God for this far I have come. He has blessed me with good health and power to overcome all the obstacles that I have encountered. Isaiah 26; 12- Lord, you establish peace for us; all that we have accomplished you have done for us.

TABLE OF CONTENTS

LIST OF TABLE

LIST OF FIGURES

ABREVIATIONS, SYMBOLS AND ACRONYMS

ARS	Acute radiation syndrome
ADC	Analogue to Digital Converter
A_D	Activity of daughter radionuclide
A_P	Activity of parent radionuclide
$Bqkg^{-1}$	Becquerel per kilogram
$CdWO_4$	Cadmium Tungsten (II) Oxide
CsI(Tl)	Thallium activated Cesium Iodide
CsI	Cesium Iodide
CsI(Na)	Sodium activated Cesium Iodide
DNA	Deoxyribonucleic Acid
D	Dose
EC	European Commission
EPA	Environment Protection Agency (USA)
EU	European Union
eV	Electron volt
HBRA	High Background Radiation Area

FWHM	Full Width at Half Maximum
GOK	Government of Kenya
IAEA	International Atomic Energy Agency
ICRP	International Commission on Radiological Protection.
KRPB	Kenya Radiation Protection Board.
LET	Linear energy transfer.
MCA	Multichannel Analyzer.
$mSvy^{-1}$	Millisievert per year
NaI	Sodium Iodide.
NaI (Tl)	Thallium activated Sodium Iodide Detector.
$nGyh^{-1}$	Nano gray per hour.
N_D	Daughter radionuclide
NCI	National Cancer Institute (Kenya).
NCRP	National Council on Radiation protection (USA).
NORM	Naturally occurring Radionuclide Material
N_P	Parent radionuclide
RBE	Relative biological effectiveness.
Sv	Sievert

UNSCEAR	United Nation Scientific Committee on the Effects of Atomic Radiation
WHO	World Health Organization
W_R	Radiation weighting factor
ZnS(Ag)	Silver activated Zinc Sulphide
α	Alpha particle
β	Beta particle
γ	Gamma ray

ABSTRACT

Natural radioactivity levels and radiation risks due to construction sand mined from Tharaka region of Tharaka-Nithi County in Kenya has been measured. The region is mostly rocky with majority of rocks being volcanic rocks and sedimentary rocks of volcanic origin; the area is occupationally characterized by sand mining for construction purposes within the County and also in some parts of the neibouring Meru and Embu Counties. The sand is mined along the river banks and also gullies that carry sand from withered rocks within the county. High concentrations of ^{238}U, ^{232}Th and ^{235}U are associated with soils that are developed from acidic magmatic rocks (igneous rocks).The goal of this study was to analyze the level of radiation exposure associated with construction sand from Tharaka region. The activity concentration levels of natural radionuclide (uranium, thorium and potassium) in the sand samples were analyzed using NaI(TI) gamma ray spectrometer. The associated radiological parameters (radium equivalent activity, dose rates, external hazard and internal hazard indices) were calculated based on the activity obtained. The results of the naturally occurring radionuclide were as follows; ^{40}K ranged from 32 ± 2 to 2662 ± 122 $Bqkg^{-1}$ with a mean value of 1069 ± 46 $Bqkg^{-1}$, ^{238}U ranged from 19 ± 1 to 269 ± 13 $Bqkg^{-1}$ with a mean value of 98 ± 4 $Bqkg^{-1}$, ^{232}Th ranged from 11 ± 1 to 114 ± 7 $Bqkg^{-1}$ with a mean value of 53 ± 3 $Bqkg^{-1}$. The mean values of activity concentration exceeded the world averages of 400 Bq/kg, 33 Bq/kg, 45 Bq/kg for K-40, U-238 and Th-232 respectively. Sand mined in Tharaka South from the gullies originating from Kijege hills and Ntugi hills were found to have elevated activity concentration especially uranium and thorium while that from Tharaka North was found to have high levels of potassium and low levels of thorium and uranium. Generally most of the samples contained elevated values of activity concentration of potassium. The hazard indices were computed and used to determine the suitability of the sand for building in the context of radiological hazard posed. Radium equivalent activity varied from 50 ± 3 to 461 ± 20 $Bqkg^{-1}$ with a mean value of 256 ± 13 $Bqkg^{-1}$, only four samples exceeded the recommended limit of 370 Bq/kg. External and Internal indices varied from 0.14 ± 0.01 to 1.23 ± 0.05 with a mean value of 0.69 ± 0.04 and 0.19 ± 0.02 to 1.80 ± 0.06 with a mean value of 0.95 ± 0.05 respectively. The outdoor absorbed dose rate calculated ranged from 22.79 ± 1.39 nG/h to 221.57 ± 9.52 nG/h with a mean of 120.99 ± 6.07 nG/h while indoor absorbed dose rate ranged from 31.15 ± 1.88 nG/h to 308.77 ± 13.20 nG/h with a mean of 166.67 ± 8.31 nG/h, the mean values were above the world averages of 54 nG/h and 84 nG/h respectively. The mean annual effective dose rate indoor and outdoor annual effective dose was 0.61 ± 0.06 mSv and 0.30 ± 0.02 mSv which was slightly above the world averages of 0.41 and 0.07 respectively but below the maximum dose constraint of 1 mSv/y to the public set by ICRP, 2005. Construction sand from the region can therefore be used without posing any danger to the public.

CHAPTER ONE

INTRODUCTION

1.1 Background to the study

Over the years, environmental pollution caused by radiations from natural, manmade or occupational sources has increased (UNESCEAR, 2000). There are two main contributors to natural radiation exposures; cosmic radiation and terrestrial radiation. Radiation exposure from natural sources accounts for 85% of the annual human radiation dose (http://www.world-nuclear-news.org, 2014). Table 1.1 shows the percentage contribution to human exposure due to radiation from different sources.

Table 1.1: Exposure percentage contributions to human due to radiation from different sources. (http://www.world-nuclear-news.org, 2014).

Source	Percentage
Radon (natural)	42%
Buildings and soil (natural)	18%
Cosmic (natural)	14%
Food/Drinking water (natural)	11%
Medicine (manmade)	14%
Nuclear industry (manmade)	1%

The three main types of cosmic radiation that are important to human exposure are; galactic cosmic radiation, solar cosmic radiation and radiation from earth's radiation

belts (UNSCEAR, 2008). Life on earth is shielded from these cosmic radiations by 10,000 kg/m^2 thick air layer and the earth's magnetic field (UNSCEAR, 2000). Annual effective dose rates from cosmic rays depends more on altitude and less on latitude. On the ground, muons are the dominant component of cosmic rays due to their high energy but as the altitude increases, electrons become an important contributor to the dose rate. At sea level the average absorbed dose rate and average annual effective dose rate is 31 nGy/h and 0.27 mSv/y respectively belts (UNSCEAR, 2008).

Terrestrial radiation is from naturally occurring radionuclides (NORMS) also referred to as primordial radionuclides present in various degrees in all environments. Only radionuclides with half-lives comparable to the age of the earth exist in sufficient quantity to contribute significantly to population exposures. Exposure to terrestrial radiation can be classified into internal and external exposures. Internal exposure is due to gamma radiation from NORMS affecting internal organs like the lungs while external exposure is caused by the gamma radiation interacting directly with externals organs like the skin. External exposures can either be indoor or outdoor while internal exposure can either be by inhalation or ingestion. Terrestrial exposure to naturally occurring radionuclides is mainly gamma radiation from ^{238}U and ^{232}Th series and from ^{40}K. ^{226}R which is a daughter of ^{238}U is normally used in the place of ^{238}U since under secular equilibrium their rate of radioactive emission is the same. Other terrestrial radionuclides are ^{235}U, ^{87}Rb, ^{138}La, ^{147}Sm and ^{176}Lu but they exist in low levels hence their contribution to doses in human is small (UNSEAR 2000). The natural percentage abundance of ^{238}U is 99.28% and ^{235}U is 0.71% hence the low contribution of ^{235}U to

very small dosage (Merrie and Thomas 1997). The radionuclides can be absorbed in plants which comprise a major source of food for humans and animals. The radionuclides can also infiltrate water sources such as lakes, oceans, rivers and streams where they are consumed by humans and animals. Ingestion intake of natural radionuclides depends on the consumption rates of food and water and also on the radionuclides concentration. Concentrations of naturally occurring radionuclides in food vary with background levels of activity concentrations, climatic and agricultural conditions of the place (UNSCEAR, 2000).

Radon and its short lived decay products in the atmosphere are the leading contributors to human exposure from natural sources (UNSCEAR 2000). Radon is formed in the decay chain of naturally occurring primordial radionuclides ^{238}U, ^{232}Th and ^{235}U present in the earth's crust. When radon is formed, it may diffuse from the rocks and soils to enter the atmosphere. The extent at which radon will diffuse into the atmosphere depends on the type of rock, soil matrix, water content and meteorological factors (UNSCEAR, 1993). Indoor radon in buildings is released from radium trapped in mineral grains of the construction materials.

All building materials contain various amounts of natural radioactivity. Materials derived from rocks and soils may contain natural radionuclides of ^{232}Th, ^{238}U and ^{40}K (EC, 1999). High concentrations of potassium, uranium and thorium are with soils that are developed from acidic magmatic rocks (igneous rocks) and clay. Natural environment radioactivity therefore depends on geology of the place (Adel, 2004).

Indoor exposures to gamma radiation depend on the materials used in construction and also on the time spend indoors. For wooden houses the indoor exposures are comparable to outdoor exposure (UNSCEAR, 2000). In a massive house made of different building materials like stone, sand, concrete and cement, indoor activity concentration from the radionuclides are high but at the same time the building is shielded from outdoor radiation (EC, 1999). The world average activity concentration of K-40, U-238 and Th-232 in the environment is 420 $Bqkg^{-1,}$ 33 $Bqkg^{-1}$ and 45 $Bqkg^{-1}$ respectively (UNSCEAR, 2008). Some construction material can cause substantial radiation exposure if they contain elevated levels of naturally occurring radionuclides (Bendibbie *et al*., 2013).

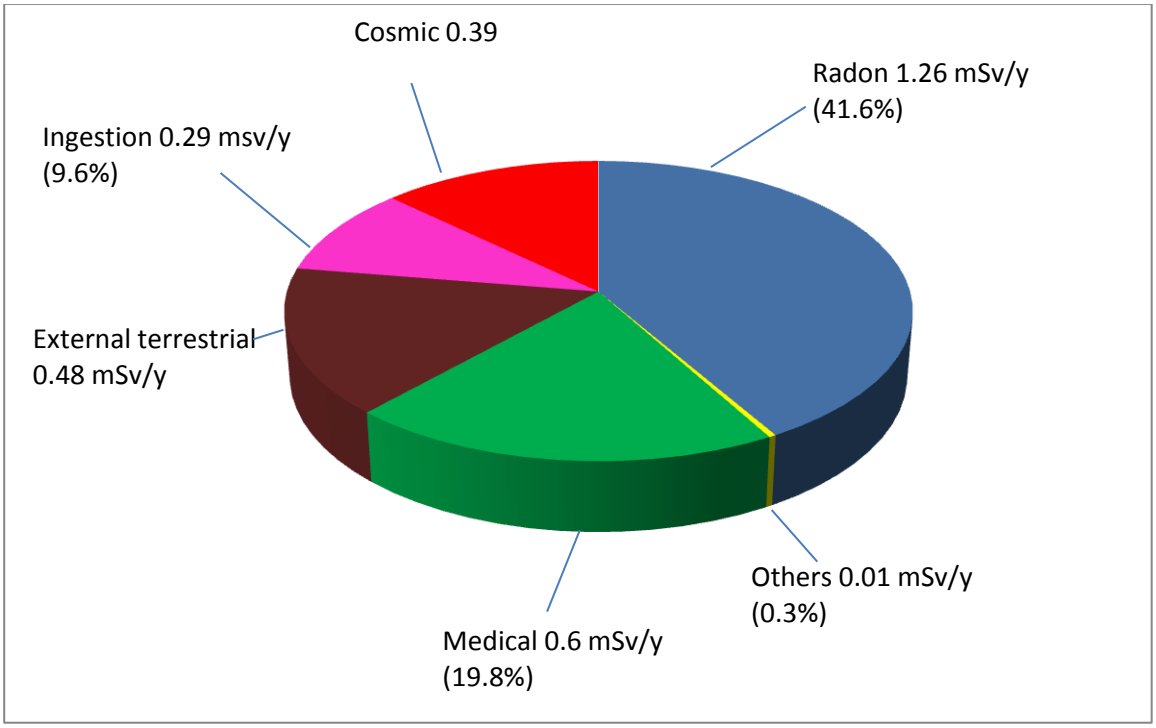

Figure 1.1: Typical contributions to public exposure from different sources to annual effective dose rates in humans (USCEAR, 2008

Some countries have laws that govern the kind of building materials to be used depending on the levels of activity concentrations of natural radionuclides in the materials. European commission has set guidelines on the recommended levels of radionuclide concentration in building materials so as to limit exposure levels (EC, 1999). Figure 1.1 shows a typical contribution from different sources to annual effective dose rates in humans.

1.2 Geology of Tharaka region

Tharaka Nithi County is located North- East of Nairobi, 175 km from the city and has a total area of about 2662 square km including the forest which covers 360 square km. It lies between latitude 00^{o} 07' and 00^{o} 26' south and longitude 37^{o} 19' and 37^{o} 46' east. The County border with Meru County to the north and north east, Kitui county to the east and south east and Embu County to the south and south west. It borders Mount Kenya forest to the western which is the source of permanent rivers that flows within the county. The permanent rivers that flow from Mount Kenya through Tharaka region are rivers Ruguti, Sagana, Thanantu, Kathita, Thuci, Maara, and Mutonga. All these rivers drain into Sagana River on the lower parts of the county.

The region forms the basement of Mount Kenya where all the remaining rocks from volcanicity are found at below 914 m (GOK, 1985). It consists of granites and gneiss rocks, usually of high quartz content yielding sandy soils. The area is characterized by different types of rocks, majority of them are volcanic rocks or sedimentary rocks of volcanic origin. The rocks in the basement system falls into four classes; schist,

psammitic rock, migmatites and intrusives (Schoeman, 1951). The schist in the region consists of appreciable amounts of potash feldspar and quartz and also other minerals like iron hydrates and biotites. The psammitic rocks are the gneiss and the quartzite. Some quartzite have high silica content and minute iron ore grains while the gneiss have high quartz content and iron ore grains. Granitic metasomatism have played a dominating role in the area. Much of the migmatite in the area are in an advanced stage of granitisation. As granitisation advances, there appears to be a general tendency for banding to become less distant with relative increase of potash feldspar and the rocks progressively assume aspect of granitic gneiss. The rocks hence become progressively lighter with advanced granatization due to increase in introduced potash felspar and quartz. The order of formation of minerals in the migmatites is mafic, accessory minerals, quartz and potash feldspars (Schoeman, 1951). The intrusives in the region are granites of volcanic origin and pegmatites. The pegmatites are of potash and soda type and contain other minerals such as quartz, mica and iron while the granites are from crystallized magmatic melt and contain primary minerals such as quartz, potash feldspar, biotite and iron ore together with other secondary minerals (Schoeman, 1951). This is in agreement with Kanoti report (2001) who recorded a high amount of potassium oxides and iron oxides in some rocks in the region. The lowlands usually receive little rainfall which does not adequately compose this parent material.

Tharaka region which is in the southern part of the county is characterized by a number of hills the major ones being Kijege and Ntugi hills. During rainy season semi-permanent rivers flow from the hills causing the rocks to wither forming sandy soils.

Mining of construction sands takes place in both permanent and semi-permanent rivers in Tharaka region of the county. Quality construction sand is mined in Igamba ng'ombe, Tharaka south and Tharaka north which are all part of Tharaka region. Tharaka south is more hilly compared to the other two regions hence is characterized by many gullies which carry sand from the hills during rainy seasons. Not all sand found here is harvested for construction this is because of its silt, salt and iron content, a good example is the large amount of sand found on a fifteen meter wide Gituma gully that carry the water and sand from the hills into Sagana River around Kibuuka area. The sand in this gully is not viable for construction due to its high iron content (Mutembei, 2013). More sand is mined on gullies than on river banks because of its quality and abundance. More sand is mined in Tharaka south than the other two regions with the least sand mining taking place in Igamba Ng'ombe due to its abundance and quality.

The colors of the sands vary depending on the type of the parent rock. It range from dark brown for the sand whose parent rock is gabbro, reddish brown, yellowish brown and pale brown for the sand whose parent rock is sand stone, quartzite, feldspar and gneiss.

1.3 Statement of the research problem

For many decades Tharaka Region has been the biggest source of sand used for construction in Tharaka-Nithi and Meru Counties. The area is characterized by different types of rocks, majority of them are volcanic rocks or sedimentary rocks of volcanic origin which upon weathering yield sandy soil. High concentrations ^{238}U, ^{232}Th and ^{40}K are associated with igneous rocks (UNSCEAR, 2000).

Radiation exposure has been associated with many forms of leukemia and with cancers of many organs such as lung, breast and thyroid (UNSCEAR, 2000). Cancer is the third killer disease causing 7% of the total national mortality every year in Kenya (GOK, 2011). In Kenya about 28,000 new cancer cases are reported annually and the resultant mortality rate is above 22,000 (GOK, 2011). According to world health organization, cancer accounted for 7.9 million (13%) deaths worldwide in 2009 with 70% of the deaths occurring in low and middle income countries. It is projected that 15.5 million people will be diagnosed and 12 Million will die of cancer worldwide in the year 2030 (WHO, 2002). This research seeks to fill the gap in determining if the radiation exposure levels in the construction sand pose any harm to the public; the miners and the inhabitants of the houses built using the sand.

1.4 Objectives

1.4.1 General objective

The main objective of this research is to analyze the quantity of radioactive emissions present in construction sand from Tharaka region of Tharaka-Nithi County so as to know if the levels are acceptable for safe usage without posing any danger to the public.

1.4.2 Specific objectives

i. To determine the activity concentration of the naturally occurring radionuclides ^{232}Th, ^{238}U, ^{40}K and their daughter radionuclides in sand samples collected in various locations around Tharaka-Nithi County.

ii. To estimate the radiation absorbed dose rates in air and annual effective dose rates from gamma rays emitted by sand samples.

iii. To determine the radium equivalent activity, external and internal hazards indices of the sand.

1.5 Rationale of the research project

Studies on natural radiation from building materials have received worldwide attention leading to intensive surveys in many counties. A number of studies on natural radioactivity contained in building materials have been conducted in Kenya (Mustapha, 1999; Achola, 2009; Shikali, 2013; Chege, 2014). Despite the continued use of the sand from Tharaka region in construction, no tangible knowledge is available about the possible radiological hazard levels and dangers associated with it. Measurement of natural radioactivity is crucial in implementing perceptional measures whenever the source is found to exceed recommended limit (Kinyua *et al.*, 2011).

Gamma ray spectrometer provides a reliable method for measuring radiation from naturally occurring radionuclides. The data obtained in this research will be used to create public awareness on the possible consequences of radiation exposure and also provide baseline data for future researchers. It is also expected that this research will give useful information to governmental and non-governmental organizations and also scientific committees like KRPB, NCI, WHO, EPA and UNSCEAR among others; this will help in policy formulation regarding environment and public health.

1 .6 Hypotheses

The concentration activity of radionuclides in the construction sand from this region is expected to be high. This could be attributed by the following factors;

i. The region falls on lowlands where agriculture chemicals and fertilizers are deposited upon being washed away from upper agriculture highlands.

ii. The area is characterized by different types of rocks, majority of them are volcanic rocks or sedimentary rocks of volcanic origin which upon weathering yield sandy soil. High concentrations ^{238}U, ^{232}Th and ^{40}K are associated with igneous rocks (UNSCEAR, 2000).

CHAPTER TWO

LITERATURE REVIEW

2.1 Studies on radiation exposure from terrestrial radionuclides

Around the world levels of terrestrial radiation vary from place to place depending on the geology of the place. In Kenya and around the world a number of studies have been carried out to assess the level of activity concentrations and the associated radiological hazards. The average radium concentrations of ^{226}Ra, ^{232}Th and ^{40}K in the earth's crust are 33, 45 and 400 Bq/kg. Elevated values of levels of natural radionuclides causing annual dosage of several mSv have been identified in some regions around the world (UNSCEAR, 2000 and UNSCEAR, 1993).

A research conducted to determine the levels of radionuclide in Kenyan coastal ecosystem revealed that the levels of radionuclides ^{226}Ra, ^{232}Th, and ^{40}K in the samples were within the acceptable limits (Hashim *et al.,* 2004). Studies to assess the radioactivity in sub surface soils around the proposed site for titanium mining in Kenya indicated that the levels of radionuclide concentration posed no harm to humans (Osoro *et al.,* 2011). In Kenya high background radiation areas include Mrima hills in Coastal Kenya, Homa Mountain and Buru hills among others. A study conducted in lambwe east, south western Kenya showed that the mean estimated annual external effective dose rates due to the rocks and soil was 5.7 mSv/y. This is Five times the recommended limit of 1 mSv/y. This region was thus considered a high background radiation Achola (2009). Mangala (1987) performed elemental analysis of samples from Mrima hills and found high concentration of thorium and rare earth metals. A ground survey of the

same area was done by Patel (1991) and annual doses as high as 106 $mSvy^{-1}$ was reported. He also reported the presence of weathered carbonatites in the region which resulted into such high doses. At Homa Mountain which is a carbonatite complex a study was done on some soil and rock samples. It indicated outdoor absorbed dose rate in air of 154.8 nG/h to 2280.6 nGy/h which is too high compared to the world average of 54 nG/h (Otwoma *et al*., 2013).

There are few places in the world known to be high background radiation areas due to geological and geochemical properties in the region (UNSCEAR, 2000). Very high background areas have been reported at beaches in Brazil (Viega *et al*., 2006; Danilo *et al*., 2013); Guangdong province of china (Wei *et al.,* 1993); Ramsar in Iran (Sohrabi., 1990; Karama, 2002); south west coast of India (Sunta, 1993) among many other regions around the world (UNSEAR, 2000). In south west coast of India large monazite deposits have been reported. The outdoor absorbed dose rates of between 5-6 mSv/y and individual doses of up to 32.6 mSv/y have been reported (Sunta 1993). A survey in high background radiation area of Ramsar in Iran by (Sohrabi) 1990 indicated indoor and outdoor absorbed dose rates of between 70 nGy/h to 17000 nGy/h which is extremely high. Annual effective dose rates of up to 98.3 mSv/y were recorded in the same area. The high radioactivity levels are due to the geology of the place. Underground water dissolves radium in uraniferous igneous rock and carries it to the surface through the hot springs. Some radium precipitates into travertine, a form of limestone and the rest diffuses into the soil where it is absorbed by the crops and mixes with drinking water. Residents in this district use this limestone as a construction

material. It irradiates the inhabitants and generates high levels of radon gas associated with lung cancer (Karama, 2002).

In a high background radiation area in Brazil large deposits of rare earth ore that form 250m above the ground have been reported. The ore contain 100, 000 tons of rare earth element and 30, 000 tons of thorium (Viega *et al*., 2006). The mean annual effective dose rate of sand beaches in Guarapari, Brazil was found to be 43 mSv/y; this is an extremely high value (Danilo *et al*., 2013). Wei *et al*. (1993) conducted a health survey in high background radiation area in Guangdong province of China. The results showed that the concentrations of natural radionuclides especially that of thorium were six times higher compared to the other neighboring regions. The source of the background radiation was found to be the nearby mountains. This was due to the rains continuously washing away the fine particles of monazite from granitic surface rocks of the mountain and depositing the same in the surrounding basin region hence the elevated levels of the background radiation.

2.2 Natural radioactivity from sand and other building materials.

In Kenya and around the world, many construction materials are collected from the environment, they include rocks, sands and other types of soils. Generally contributions from these building materials to the total doses in dwellings are small compared to those underlying bedrocks and soils unless they are extracted from high background radiation areas (Mustapha *et al*., 1997). An EC report on Radiological Protection Concerning the Natural Radioactivity of Building Materials indicated most important source of indoor

radon is the underlying soil and also building materials (EC Report 112, 1999). In the same report the EC has set Radiation Protection Principles to limit radiation exposure due to elevated levels of natural radionuclide for member countries. In many countries high radiation levels have been associated with these construction materials triggering many governments and international bodies such as EU commission, WHO and ICRP among others to adopt measures aimed at minimizing exposures due to indoor radiation. Shikali *et al.* (2014) analyzed activity concentrations of construction sand samples around the old gold mining zones in Kakamega, Kenya. The activity concentrations of the naturally occurring radionuclides in the sand samples were calculated and obtained as 128.05 Bq/kg, 98.37 Bq/kg and 756.39 Bq/kg for ^{238}U, ^{232}Th and ^{40}K respectively. The study reported annual dose rates of between 0.48 mSv/y and 0.92 mSv/y which are below recommended limit of a unity. He concluded that the sand from the area can be used safely for construction without posing any significant radiological threat to humans. Mustapha *et al*. (1997) analyzed natural activity in some building materials in Machakos, Kenya and their contribution to the indoor external doses. The materials analyzed were tuffs, phonolites, gneisses, granites, red lateritic soils and sandy soils. The phonolites were found to have an annual effective dose rate of 1.27 mSv/y which is above the recommended limit of 1 mSv/y hence it poised a radiological hazard if used as a construction material. All other materials that were analyzed were found to have a dose rate of less than unity hence making them suitable for use as a construction material. The activity concentrations of sand samples analyzed were found to be 802 Bq/kg, 11 Bq/kg and 5 Bq/kg for ^{40}K, ^{238}U and ^{232}Th respectively. The gamma dose rate and annual effective dose rate obtained was 66 nGy/h and 0.24 mSv/y respectively. This

means that construction sand in the area does not pose any harm and can safely be used as a construction material without any limitations. An elevated level of indoor radon in homes and workplaces has been reported by Mustapha (1999) and Chege (2007, 2014).

Bendibbie *et al.* (2013) performed a radiological analysis of suitability of Kitui limestone for use as a building material. The activity concentrations of ^{232}Th were below the detection limits while that of ^{238}U and ^{40}K varied from 28.3 to 47.4 Bq/kg and 87.4 and 142.6 Bq/kg respectively, the levels are below the world averages. The results showed that the radium equivalent activity for all the samples was below the recommend limit of 370 Bqkg^{-1} and all the radiation hazard indices were below a unit. From the results therefore, the limestone mined in the area can be used as building material or for manufacture of building materials without any restrictions.

In Turkey, an assessment natural radioactivity of sand used for construction in the whole country has been done (Cevic *et al.,* 2009). The activity concentrations in sand samples varied from 17 to 97 Bq/kg, 10 to 133 Bq/kg and 16 to 955 Bq/kg for ^{226}Ra, ^{232}Th and ^{40}K respectively. The analysis of the associated radiological hazards showed that sand samples do not pose any significant source of radiation hazard and are safe to be used as building materials.

Gupta *et al.* (2010) conducted a research to estimate radioactivity in building sand and soil samples in India. The variations in activity concentrations of ^{238}U, ^{232}Th and ^{40}K were found to be 45-97 Bq/kg, 63-132 Bq/kg and 492-1110 Bq/kg respectively in soil

samples while variations in sand samples were 63-65 Bq/kg, 86-96 Bq/kg and 751-824 Bq/kg respectively. The radium equivalent in most of the samples was less than the upper recommended value of 370 Bq/kg and the dose equivalent in most of the samples was within the safe limit of 1msv/yr. The minimum and the maximum values of absorbed dose, indoor annual effective dose and outdoor annual effective dose in the sand samples was found to vary from 113 to 121 nGy/h, 0.56 to 0.60 nGy/h and 0.14 to 0.15 mSv respectively. The samples were found to satisfy the safety criterion as a building material hence can be used without any limitations.

Kinsara *et al*. (2014) measured natural radioactivity in some building materials originating from a high background radiation area in Hail province, Saudi Arabia. The results showed that the highest activity concentrations were found in the fragmented granite materials and had a mean value of 194 Bq/kg, 912 Bq/kg and 1320 Bq/kg for ^{226}Ra, ^{232}Th and ^{40}K respectively. These values are too high compared to the world average. The activity concentrations of the sand samples in the region were found to vary from 19-37 Bq/kg, 107-204 Bq/kg and 135-180 Bq/kg with a mean value of 29 Bq/kg, 158 Bq/kg and 139 Bq/kg for ^{226}Ra, ^{232}Th and ^{40}K respectively. The sand recorded a mean radium equivalent of 265 Bq/kg which is below the recommended maximum limit of 370 Bq/kg making it safe for use in construction purposes.

A study was done to assess natural radiation exposure and radon exhalation rate in various samples of Egyptian building materials (Shoeib and Thabayneh 2014). The samples analyzed were cement, white cement, gypsum, granite, ceramic and hydrated

lime. The activity concentrations for ^{226}Ra, ^{232}Th, and ^{40}K, from the selected building materials, ranged from 8.2 to 288.5 Bq kg^{-1}, 3.6 to 77.8 Bq kg^{-1} and 4.1 to 1314 Bq kg^{-1}), respectively. The activity found for ^{226}Ra was the lowest for gypsum and maximum for cement bricks, ^{232}Th concentration found for cement plaster was the lowest and cement brick was the highest, ^{40}K concentration found in granite was the maximum and in white cement it was the lowest. The calculated annual effective dose rates absorbed by the inhabitants of the building from the construction materials were below 1 mSv/y except for cement bricks. This is an indicator that the materials are safe to use for construction purposes except the cement brick that recorded values above acceptable limit.

2.3 Radiation and radiobiology

Radiation is classified into two main categories, nonionizing and ionizing, depending on its ability to ionize matter. The minimum energy required to ionize an atom (ionization potential) ranges from a few electron volts for alkali elements to 24.5 eV for helium (noble gas). Ionizing radiation can be classified as either directly ionizing radiation or indirectly ionizing radiation. Directly ionizing radiation are charged particles which include electrons, protons, α particles and heavy ions. Indirectly ionizing radiation are neutral particle which include neutrons and photons; X rays and γ rays (IAEA, 2005). Photons of γ rays ionizes an atom by first releasing in the medium electrons or positrons then the released charged particles deposit energy to the medium through direct Coulomb interactions with orbital electrons of the atoms in the medium. Linear energy transfer (LET) is the rate of energy absorption by the absorbing medium and it

determines the quality of ionizing radiation beam. Gamma rays have a high penetrating power hence are considered low LET (sparsely ionizing). The demarcation between low LET and high LET is 10 keV/μm. Typical LET value of Cobalt-60 Gamma ray is 0.3 keV/μm.

The cell is composed of two main components, the nuclei that contain the DNA and the cytoplasm. When the cells are exposed to the ionizing radiation, physical effects between radiation and the molecules of the cell occur first. This is can be followed by biological damage which include; damage to the DNA, which is the most crucial target of the cell, cell death or damage to other parts of the cell (IAEA, 2005). Radiation exposures can damage living cells, causing death in some of them and modifying others. Most organs and tissues of the body are not affected by the loss of even considerable numbers of cells. However, if the number lost is large enough, there will be observable harm to organs and this may lead to death. This type of harm occurs in individuals who are exposed to radiation in excess of a threshold level. Other radiation damage may also occur in cells that are not killed but modified, this damage is usually repaired. If the repair is not perfect, the resulting modification will be transmitted to further cells and may eventually lead to cancer. If the cells modified are those transmitting hereditary information to the descendants of the exposed individual, hereditary disorders may arise (UNSCEAR, 2000).

The effects of ionizing radiation to humans can either be somatic or genetic. Somatic effects are the effects that humans suffer in their lifetime due the exposure to the

radiation. They include sterility, radiation induced cancers, human death and damage to the eye lens (IAEA, 2005). Somatic effects to ionizing radiation are classified into prompt or delayed. Prompt somatic effects are those that are felt soon after exposure to ionizing radiation for instance temporary hair loss that occur about three weeks after a dose exposure of about 400 rad to the scalp. Delayed somatic effects are felt many years after exposure and are mostly linked to the development of cancers (Atambo, 2011). Radiation induced cancer may manifest its self, decades after exposure (UNSCEAR, 2000). Genetic effects also known as hereditary effects are mutations to an individual's genes and DNA due to the ionizing radiation; they can result to birth defects of the descendants (IAEA, 2005). Pregnant women particularly in the first 20 weeks of pregnancy should avoid exposure to ionizing radiation. This is because a foetus cells are rapidly dividing hence sensitive to radiation. Pre-natal exposure to ionizing radiation may affect the child causing; childhood cancer, growth retardation, small head/brain size and mental retardation (IAEA, 2005).

Ionizing radiation falls into two categories chronic and acute dose. Acute dose is defined as large dose of more than 10 rad delivered to the whole body over a short period of time. It can result into observable symptoms within a few hours or weeks depending on the quantity of the dose (http://www.world-nuclear-news.org, 2014). Radiation sickness symptoms are apparent following acute doses of 100 rad and above. Acute whole body dosage of above 450 rad may cause death to half of the population exposed within 60 days if the victim does not receive medical attention. A good example is Chernobyl accident where 28 of the most heavily exposed died as a result of

acute radiation syndrome (ARS) within three months of the accident (http://www.world-nuclear-news.org, 2014). Chronic dose is relatively small amount of radiation received over a long period of time; it is less lethal compared to acute dose. It gives the body time to repair the damaged cells and to replace the dead or non-functioning cells with new healthy cells (UNSCEAR, 1996).

To minimize the effects of ionizing radiation to the public the principles of radiation protection is to limit dosage for public and occupational exposure however dose limits are not applicable to medical exposures.

CHAPTER THREE

THEORETICAL BACKGROUND

3. 1 Radioactive emissions

Three ionizing radiations namely alpha (α) particle, beta (β) particles and gamma (γ) rays are emitted during radioactive decay. Ionizing radiations are classified into two categories; directly ionizing and indirectly ionizing radiation. Charged particles namely alpha particle and beta particles are directly ionizing while neutral particles i.e. γ rays are indirectly ionizing. Alpha particles are helium nuclei consisting of two protons and two neutrons, giving a net positive charge. They are emitted from naturally-occurring heavy elements such as uranium and radium, as well as from some man-made transuranic elements. They are intensely ionizing but due to their low penetration power, they cannot penetrate the skin, so are dangerous only if emitted inside the body.

Beta particles are fast-moving electrons or positron emitted by many radioactive elements. They are caused by emission of excess neutrons in the atomic nucleus. When there are significantly more neutrons than protons in a nucleus, the neutrons degenerate into protons and electrons, which are ejected from the nucleus at high speeds. This increases the atomic number of the atom and also its stability. Beta emitters include strontium-90, potassium-40, technetium-99, tritium, and carbon-14. They are more penetrating than alpha particles, but easily shielded – the most energetic of them can be stopped by a few millimeters of wood or aluminium. They can penetrate a little way into human flesh but are generally less dangerous to people than gamma radiation. Exposure produces an

effect like sunburn, but which is slower to heal. The weakest of them such as from tritium, are stopped by skin or cellophane. Beta-radioactive substances are also safe if kept in appropriate sealed containers.

Gamma rays are high frequency electromagnetic waves. They have the smallest wavelength and are the most energetic in the electromagnetic spectrum. They are emitted in many radioactive decays and may be very penetrating, so require more substantial shielding. Gamma rays are the main hazard to people dealing with sealed radioactive materials used, for example, in industrial gauges and radiotherapy machines. Radiation dose badges are worn by workers in exposed situations to detect them and hence monitor exposure (IAEA, 2005). All of us receive about 0.5-1 mSv per year of gamma radiation from cosmic rays and from rocks, and in some places, much more (UNSCEAR, 2008).

3.1.1 Production and health effects of gamma rays

Gamma rays were discovered in 1900 by a French physist known as Paul Villard. Gamma rays are often produced alongside alpha-particles and beta-particles. When a nucleus emits alpha particle or a beta particle, the daughter nucleus is at times left in an excited state. To attain its ground state, it emits one or several gamma photon. An example of this is transition of excited $^{60}_{28}\text{Ni}^{**}$ into a stable $^{60}_{28}\text{Ni}$ through emission of two gamma rays of energies 1.332 MeV and 1.170 MeV as shown in figure 3.1.

Gamma rays have very high penetrating power. The most biological damaging forms of gamma radiation occur in the gamma ray window, between 3 MeV to 10 MeV. Higher energy gamma rays are less harmful because the body is relatively transparent to them. Gamma rays are better absorbed by materials with a higher density and atomic number. Higher energy gamma rays require a thick shielding material and lead is the most preferred due to its compactness. The quality of a shielding material is determined by its ability to reduce the intensity of a radiation by half (IAEA, 2005).

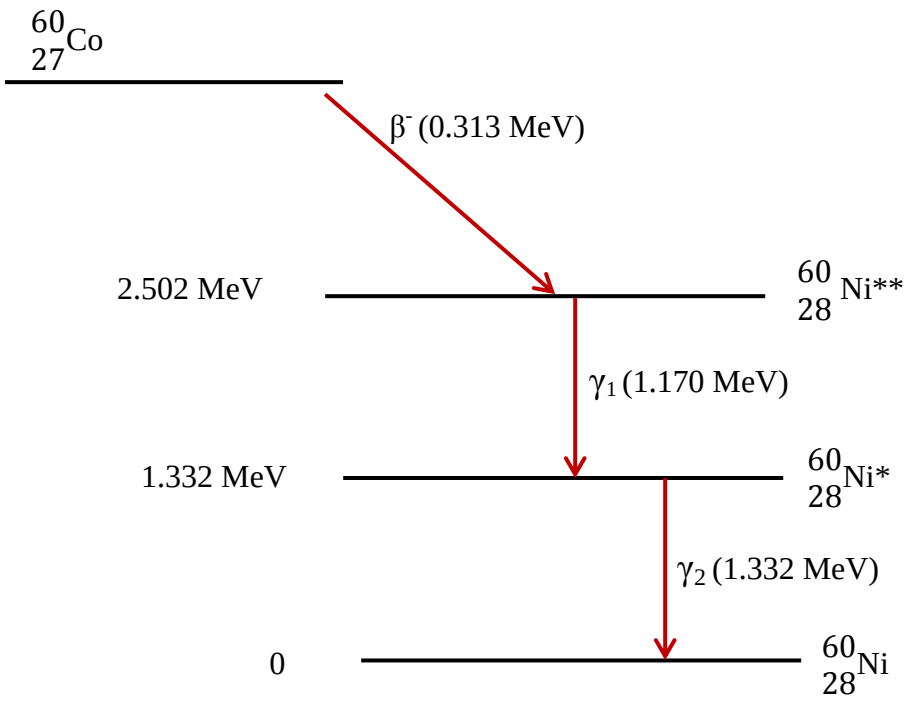

Figure 3.1: A diagram illustrating the decay scheme of ^{60}Co decay.

3.1.2 Units of radiation exposure

The measure of ionizing ability of gamma radiation is called exposure. The biological effects of an ionizing radiation depend on the amount of energy it deposits on a human tissue. Absorbed dose, D is the fundamental physical quantity in radiological protection. It is defined as the amount of energy absorbed per unit mass of the tissue and its units is called the Gray (Gy). At a given absorbed dose, the actual value of energy imparted in a cell is given by the product of frequency of energy deposition events and the value of energy deposited in each event (ICRP, 2005). One Gray is equal to one Joule of radiation absorbed per unit kilogram of a tissue (Mudd, 2008). The rad is the corresponding traditional unit (obsolete), equal to 0.01 J deposited per kg i.e. 100 rad = 1 Gray.

Equivalent dose (H) is calculated from the absorbed dose using conversion factors. It is defined as the measure of biological effect of radiation on human tissue. The SI unit of equivalent dose is the Sievert (Sv). The rem is the traditional unit of equivalent dose, 1 Sv = 100 rem.

$$H = D \times W_R \qquad (3.1)$$

Where, W_R is the radiation weighting factor. Values of W_R are based upon the relative biological effectiveness (RBE) of various radiations for stochastic effects, especially compared with the effects of γ rays at low doses (ICRP, 2005).

3.2 Secular equilibrium

Thorium and uranium decay chains provide radionuclides of significance in NORM. Secular equilibrium is a condition in which the decay rate of parent radionuclide is equal to that of daughter radionuclide. This can only occur if the half-life of the parent is much longer compared to that of daughter such that there is no significant decay during the time interval of interest. If the samples are left undisturbed for a long period of time, the decay rate of the parent radionuclide and hence the rate of production of the daughter radionuclide is constant. This is because the time scale under consideration is very small compared to the half-life of the parent radionuclide. Under secular equilibrium, each member of the decay chain has the same activity due to the fact that the quantity of the daughter radionuclides builds up until the number of its atoms decaying per unit time becomes equal to the number being produced per unit time as shown in figure 3.2. In this case the activity of the daughter radionuclide can be determined by the activity of the parent radionuclide. By taking N_D and N_P to be the initial number of atoms of daughter and parent radionuclide with the corresponding activities A_D and A_P respectively, the idea of secular equilibrium can be explained using decay laws;

$$\frac{dN_D}{dt} = \lambda_P N_P - \lambda_D N_D \tag{3.2}$$

Where λ_D and λ_P are decay constants of the daughter and the parent respectively and can be calculated from half-life using the expression;

$$\lambda = \frac{In(2)}{t_{\frac{1}{2}}} \tag{3.3}$$

Decay rate of the parent is very slow hence;

$$A_P(t) = \lambda_P N_p(t) \sim A_0 \text{ (a constant)} \tag{3.4a}$$

And also

$$\frac{dN_p}{dt} \sim 0 \tag{3.4b}$$

The number of the first daughter atoms can decay away no faster than they were formed at the constant rate A_0 i.e.

$$\lambda_D N_D(t) \sim \lambda_P N_P(t) = A_0 \tag{3.5a}$$

Thus

$$\frac{dN_D}{dt} \sim 0 \tag{3.5b}$$

Under secular equilibrium we have;

$$\frac{dN_p}{dt} \sim \frac{dN_D}{dt} \sim 0 \tag{3.6a}$$

Or equivalently;

$$A_0 \approx A_P \approx A_D \quad (3.6b)$$

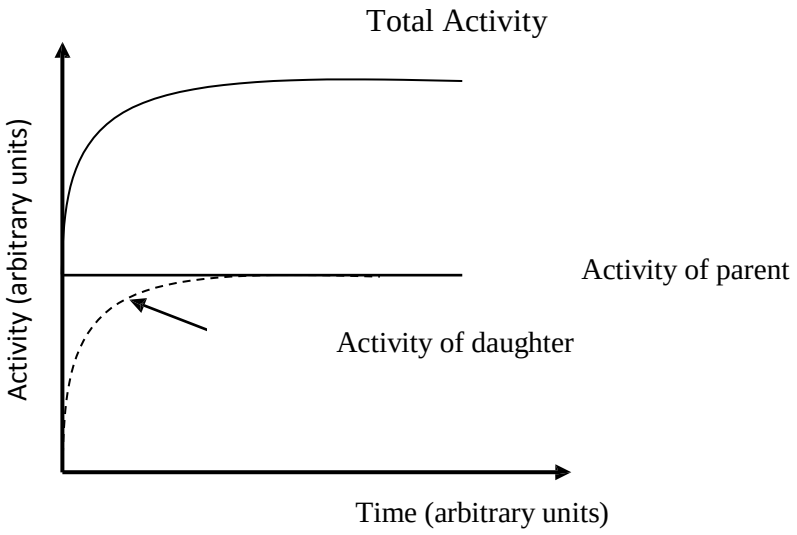

Figure 3.2: Secular equilibrium of a parent and daughter radionuclide.

3.3 Interaction of gamma-ray photons with matter

Interaction between gamma rays with matter results into reduction in its intensity. This is due to absorption of all or part gamma ray photon by the particles of the material. The intensity of the photon beam varies in matter according to the exponential absorption law given by;

$$I = I_0 \exp(-\mu x) \quad (3.7)$$

where, I_0 is the intensity of the incident radiation at a depth of x into the absorbing material. μ is the linear attenuation coefficient; it is the probability per unit length that

the photon is removed from the beam (Knoll, 1999). Interaction between a photon and the absorber depends on the energy of the photon and the atomic number of the attenuator; it can occur with a free electron, with the field of the nucleus or with a tightly bound electron. The interaction of gamma ray photon is through three mechanisms; photoelectric absorption, pair production and Compton scattering. For a given photon (hν) the attenuation coefficient, μ is the sum of the coefficients for individual photon interactions.

$$\mu = \sigma \text{ (Compton)} + \tau \text{ (photoelectric)} + K \text{ (pair production)} \quad (3.8)$$

Linear attenuation coefficient varies with the density of the absorbing material hence mass attenuation is widely used because of that limitation, it is defined as;

$$\frac{\mu}{\rho} = \frac{\sigma}{\rho} + \frac{\tau}{\rho} + \frac{K}{\rho} \quad (3.9)$$

where, ρ is density of the absorbing material.

3.3.1 Photoelectric absorption effect

Interaction between a gamma ray photon of sufficient energy and matter causes an electron to be ejected from the absorbing material as shown on figure 3.3. The incident gamma ray photon interacts with electron of the atom and causes the photon to completely disappear. It occurs only on bound electrons since the free electron cannot

absorb a photon and conserve momentum. A very small amount of recoil energy remains in the atom for momentum conservation. The highest probability of photoelectric effect is in the K-shell electrons since they are the most tightly bound. Photoelectric absorption takes place for photons with energies of a few electron volts to over 1 MeV. The ejected electrons have kinetic energy given by;

$$KE = h\nu - E_b \tag{3.10}$$

Where hν is the energy of the incident gamma rays and E_b is the binding energy.

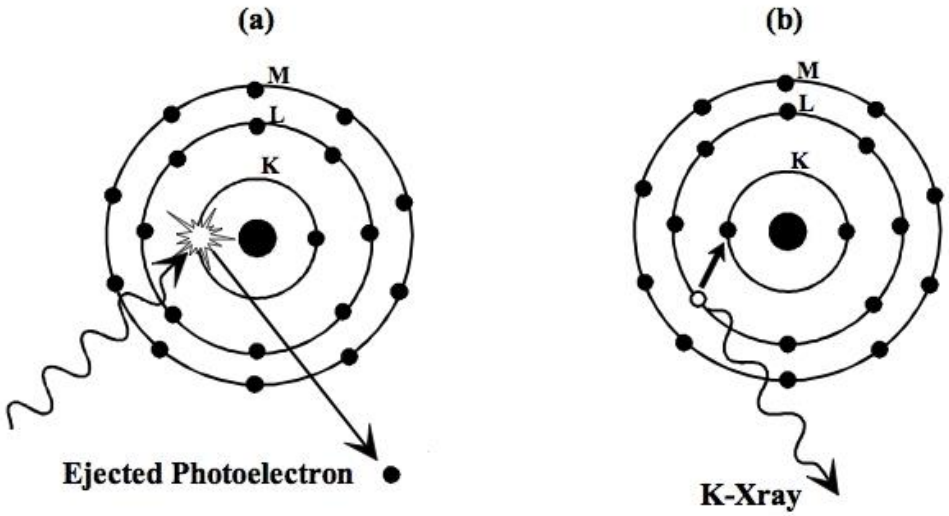

Figure 3.3*:* Schematic diagram of photoelectric absorption (https://enwikibooks.org/wiki).

The vacancy created in one of the bound shell is quickly filled through a free electron capture from a media or arrangement of electron from other shells of the atom. The

binding energy appears as the characteristic X-rays emitted in coincidence with the photo electron. The excited atom may also de-excite by the emission of an outer electron also known as Auger electron. Most of the X-rays as well as the Auger electron are absorbed by the detector. Photoelectric effect is most dominant at low energy γ or X-ray photons and high atomic number materials. The probability of photo electric absorption (also known as cross-section τ_{PE}) is given by equation 3.11 (Grupen, 1996).

$$\tau_{PE} = \text{constant} \times \frac{Z^n}{E_\gamma^{3.5}} \tag{3.11}$$

where Z is the atomic number of the absorber and E_γ is the energy of the radiation. Exponent n varies between 4 and 5 over the gamma ray energy region of interest.

3.3.2 Compton scattering

Compton scattering represents a photon interaction with an essentially "free and stationary" orbital electron. Figure 3.4 illustrates the scattering of an incident photon of energy E = hν moving with a momentum p = $\frac{h}{\lambda} = \frac{h\nu}{c}$. It occurs when the incident photon energy (hν) is much larger than the binding energy of the orbital electron. It interacts with an electron at rest having a momentum $p_e = 0$ and rest energy $E_o = m_o c^2$. Upon interaction, the gamma ray is scattered at an angle θ with respect to its original direction with momentum of magnitude $p' = \frac{h\,\nu'}{c} = \frac{h}{\lambda'}$ and energy $E' = h\nu'$. The recoil

(Compton) electron is scattered at an angle ϕ with momentum $p'_e = \frac{1}{c}\sqrt{E_e^2 - E_0^2}$ and energy $E_e = mc^2$.

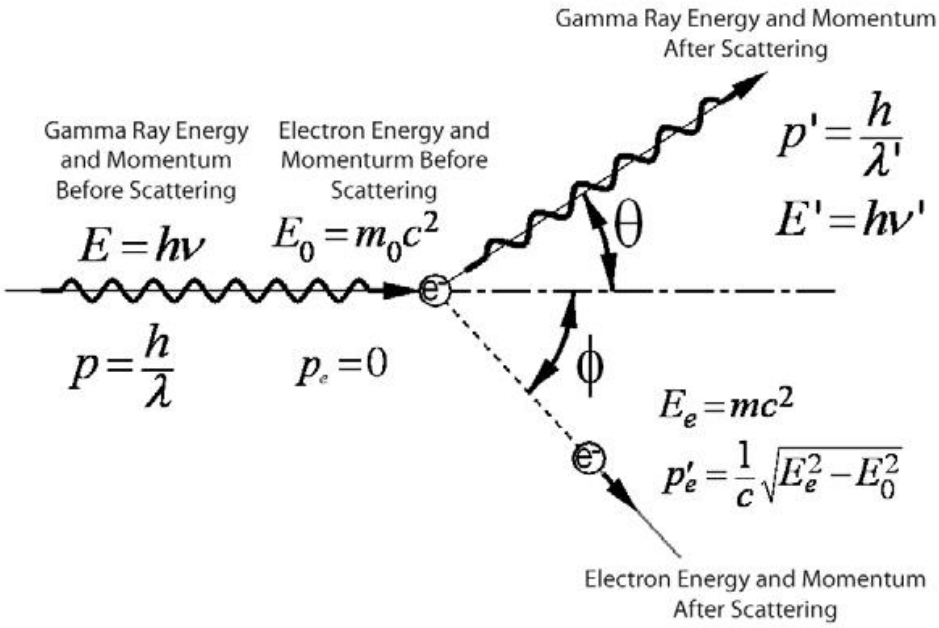

Figure 3.4: Schematic diagram of Compton scattering showing the relationship of the incident photon and electron initially at rest to the scattered photon and electron given kinetic energy (James, 2014).

The scattered photon energy and the kinetic energy of the recoil (Compton) electron in terms angles shown in figure 3.4 are given by equations 3.12 and 3.13 (IAEA, 2005);

$$h\nu' = \frac{h\nu}{1+\varepsilon(1-cos\theta)} \tag{3.12}$$

$$E_k = h\nu \frac{\varepsilon(1-cos\theta)}{1+\varepsilon\,(1-cos\theta)} \tag{3.13}$$

where $\varepsilon = \frac{hv}{m_0 c^2}$ (3.14)

The symbol ε represents the normalized incident photon energy. All angles of scattering are possible hence the energy transfer can vary from zero to a large fraction of the gamma ray energy. The maximum transfer of energy to the electron and hence the minimum energy of the scattered gamma, occurs when θ = 180°.

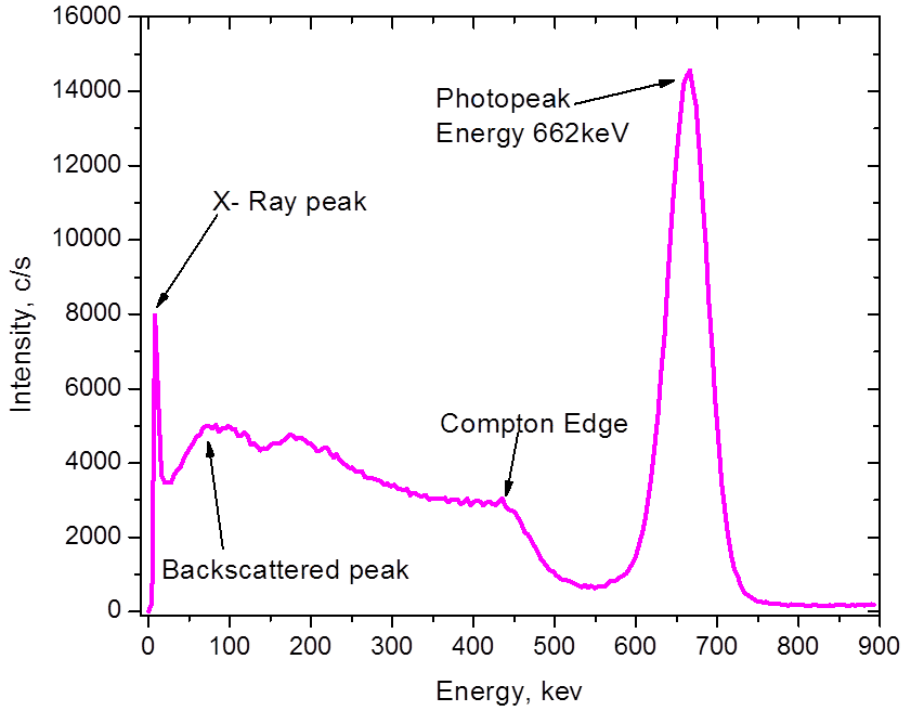

`

Figure 3.5: A typical ^{137}Cs spectrum showing Compton effect as measured in this study.

In normal situations, all scattering angles occur in a finite sized detector volume hence a continuum of energies is transferred to the recoil electron. If a head-on collision occurs,

the scattering of the incident gamma photon is towards the direction of the origin. This leads to the energy transferred to the recoil electron in a single Compton reaching a maximum value. This forms a special feature known as "Compton edge".The interaction cross-section of Compton scattering is given by (Knoll, 1999);

$$\sigma = \text{constant} \times \frac{Z}{E} \tag{3.15}$$

where Z is the atomic energy of the attenuator and E = hν, is the incident photon energy. Compton scattering is the most predominant mechanism of interaction for gamma ray energy typical of radioisotope sources.

3.3.3 Pair production

Pair production takes place in the coulomb field of a nucleus. Figure 3.6 shows that in the process, a gamma photon disappears and an electron-positron pair is produced (IAEA, 2005). The probability for pair production is zero for photon energies below the threshold energy of $2m_ec^2$ (1022 keV) and increases rapidly with increase in photon energy above the threshold. The excess energy ($h\nu$- $2m_ec^2$) is shared between the electron-positron pair as the kinetic energy. The partition of the energy to the electron and positron is symmetric at low energies ($E\gamma << 50$ MeV) and increasingly asymmetric at high energies ($E\gamma > 1$ GeV). The kinetic energy deposited to the absorber material is proportional to the incident gamma ray photon.

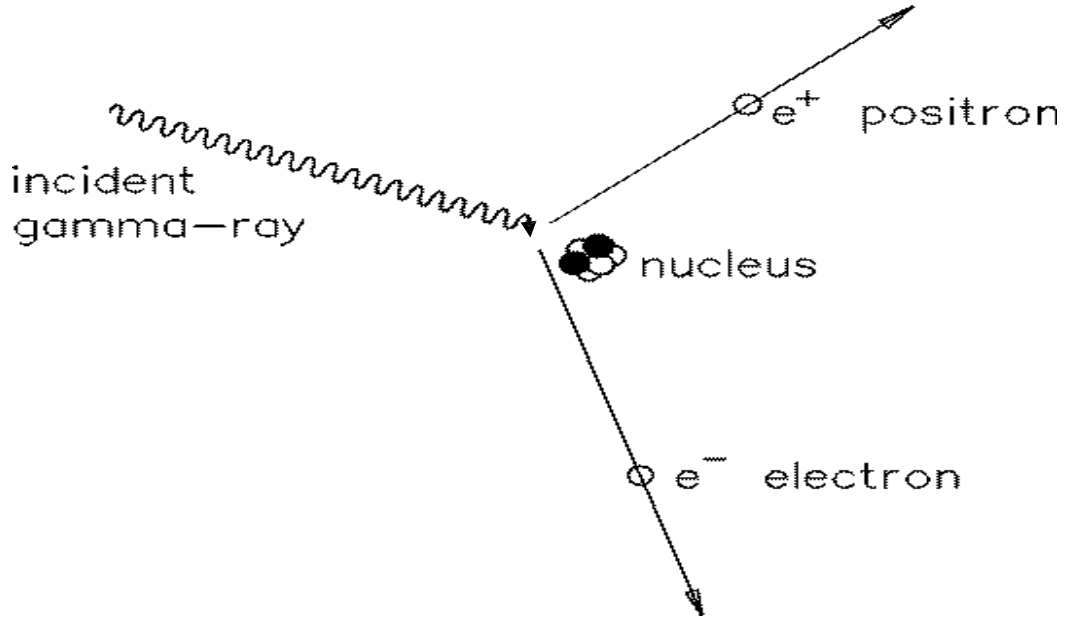

Figure 3.6: Schematic diagram of pair production process occurring in the coulomb field of a nucleus (Atambo, 2011).

The process of pair production can be explained by equation 3.16.

$$h\nu = 2m_e c^2 + E_{kin}^{+} + E_{kin}^{-} \quad (3.16)$$

where hν is the energy of the incident gamma ray photon, m_e is the rest mass of an electon. A positron can move faster and cover its range before time needed for pulse formation or it can combine with electron at especially at the end of the track. The two annihilate and results into the formation of two gamma photons of 511 keV each. The annihilation of gamma ray photon can give rise to three distinct peaks. Total absorption peak occurs when the energy of both annihilation gamma rays are deposited in the

detector, Single escape peak is recorded when one annihilation photon escapes and double escape peak is recorded by the detector when both annihilation photons escape.

Pair production is predominant at high photon energy and high z material. The cross-section for pair production process is given by (Grupen, 1996);

$$\sigma_{\text{pair}} = \frac{9}{7}\frac{A}{N_A}\ \frac{1}{X_0} \tag{3.17}$$

where N_A is the Avogadro number and A is the atomic mass. x_0 is the radiation lengths of the absorber in which pair production takes place and it is given as (Grupen, 1996);

$$x_0 = \frac{716.4A}{z(z+1)\ In(287/\sqrt{z})} \tag{3.18}$$

where, z is the atomic mass of the absorber.

3.4 Relative predominance of the individual effect

The strength of each of the three types of gamma ray interactions depends on the atomic number of the material the interaction is taking place and also the initial gamma ray energy. Figure 3.7 shows that at low energies, photoelectric effect becomes most dominant and is also enhanced by absorbers with a high atomic number while Compton Effect predominates at intermediate energies and pair production at high energies.

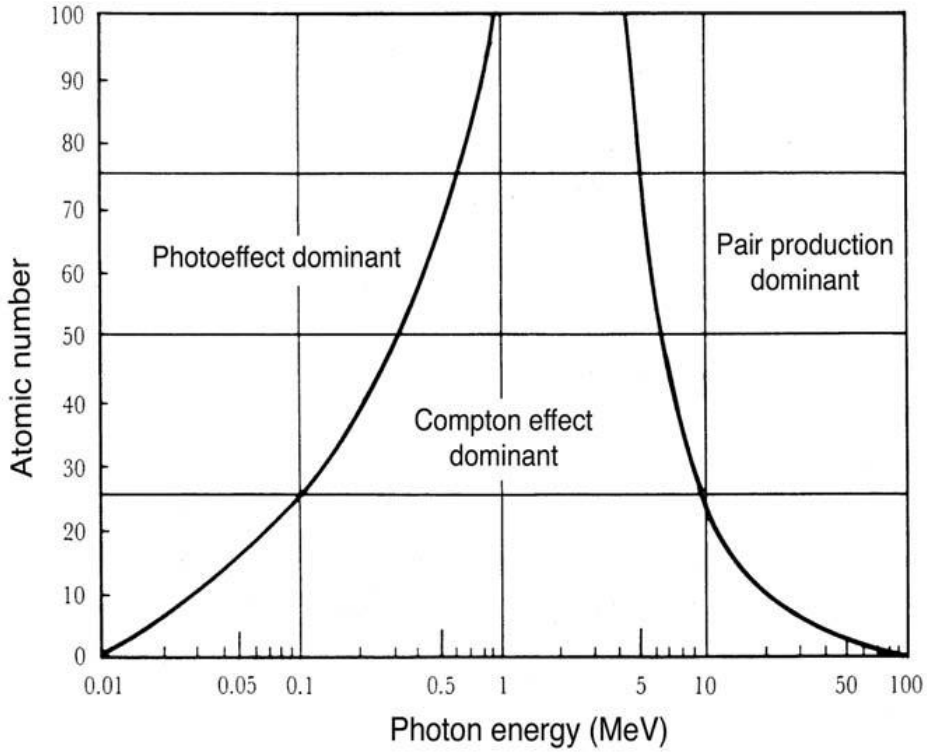

Figure 3.7: Schematic representation of the three major gamma-ray interactions (IAEA, 2005).

3.5 Scintillation Detectors

Detectors based on scintillation (light emission) are known as scintillation detectors, they emit light when radiation interacts with the atoms in the crystal. The intensity of the light produced is directly proportional to energy deposited by the radiation. Some examples of inorganic scintillators are alkali halide: NaI(Tl), CsI(Tl), CsI(Na) other slow inorganics that include $CdWO_4$ and ZnS(Ag). The properties of scintillation materials required for good detectors are transparency, availability in large size and large light output proportional to gamma ray energy. Relatively few materials have

good property for detectors, Thallium activated NaI and CsI crystals are commonly used.

The scintillation mechanism depends on the structure of the crystal lattice. Incident particles can transfer energy to the lattice by creating electron-hole pair or taking electrons to higher levels below the conduction band. Electron-hole bound states (excitations) moving through a lattice can emit light when hitting an activator, also recombination of electron-hole pairs may lead to emission of light. In pure inorganic crystals lattice such as NaI, electrons are allowed to occupy selected energy bands. The range of energies in which electrons can never be found in pure crystals is called band gap (forbidden gap). Photon energy absorbed in the pure crystal can elevate electrons from valence band to conduction band leaving a gap in the valence band. The inefficient process where the electron return to the valence band emitting a photon results into emission of few photons per decay in that the energy is emitted by other mechanisms.

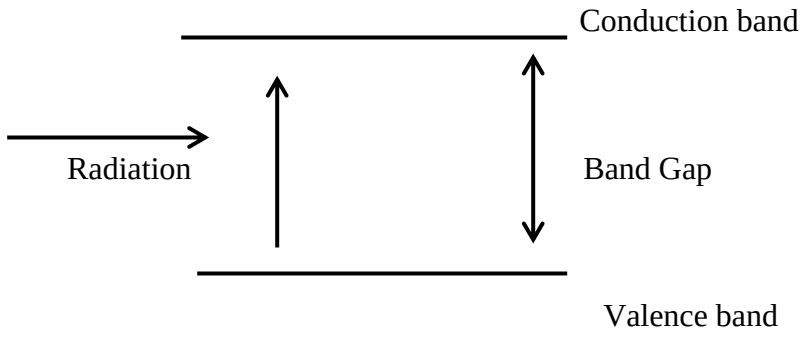

Figure 3.8a: Energy band gap structure of pure crystal inorganic scintillator.

Secondary band widths in pure crystals are such that the resulting photon is too high to lie within the visible range as shown in figure 3.8a.

Small impurities (activators) are added to the pure crystal to create special sites in the lattice at which the band structure, energy structure is modified as shown in figure 3.8b. Energy states are created within what would be the forbidden band of a pure crystal and the electron can de-excite through these levels and back to the valence band (Knoll, 1999).

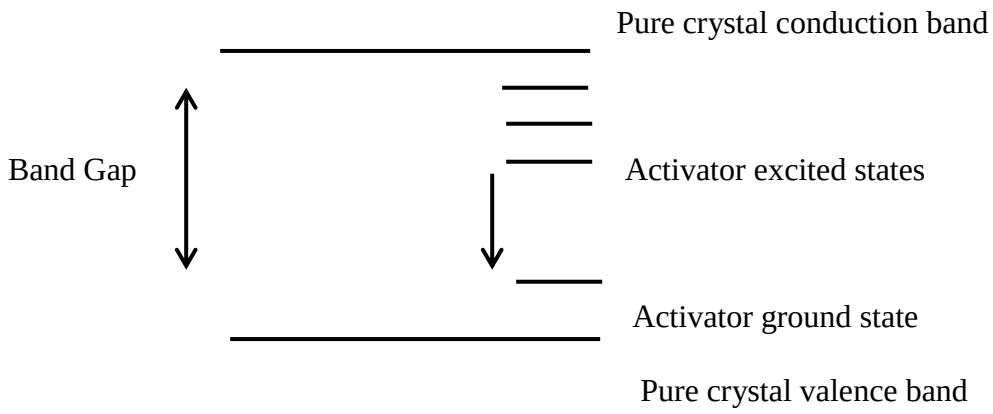

Figure 3.8b: Energy band gap structure of an activated crystalline inorganic scintillator.

3.5.1 NaI (Tl) Gamma ray Detector

The detector's working principle is based on emission of light by scintillating materials when illuminated by a gamma ray radiation. It consists of a scintillator, a photomultiplier tube and associated electronics. Photons from a radioactive source enter NaI(Tl) scintillation crystal and deposit energy either by photoelectric effect, Compton

scattering or pair production depending on the photon energy. The working of a photomultiplier is shown in figure 3.9; it consists of a photocathode, a focusing electrode and 10 or more dynodes. A photomultiplier tube takes electrical signal from photocathode and amplifies it through dynode chain by a process of electron multiplication.

The electrons are ejected from the photocathode with energy of ≈ 1 eV and are accelerated by a voltage of a few hundred volts towards an electrode. The accelerated electron has energy of a few hundred electron volts upon arrival at the electrode. This deposition of kinetic energy can result in re-emission of secondary electrons. The electrons created in the photocathode are accelerated towards the first dynode where secondary electrons are emitted. The secondary electrons are accelerated towards the second dynode by the electric field where they create secondary electrons and the process continues up to the last dynode (Knoll, 1989). The output from the photomultiplier is proportional to the energy absorbed by the scintillating material (Leo 1994). The electrons are collected by the anode at the end of the tube forming an electric pulse that is displayed by a computer. The overall gain in the photomultiplier tube is calculated using equation 3.19 (Knoll, 1989);

$$\text{Gain} = \alpha\sigma^{n} \qquad 3.19$$

where n is the number of multiplication stages, α is the fraction of electrons collected by the multiplier structure and σ is multiplication factor for a single electron. The typical

values of σ are about 5 and α approaches unity. 10 stages of multiplication therefore can result to an overall gain of 5^{10} or 10^7. The high Z of iodine in Nal gives good efficiency for gamma ray detection. A small amount of Tl is added in order to activate the crystal so that the designation is usually NaI(Tl) for the crystal.

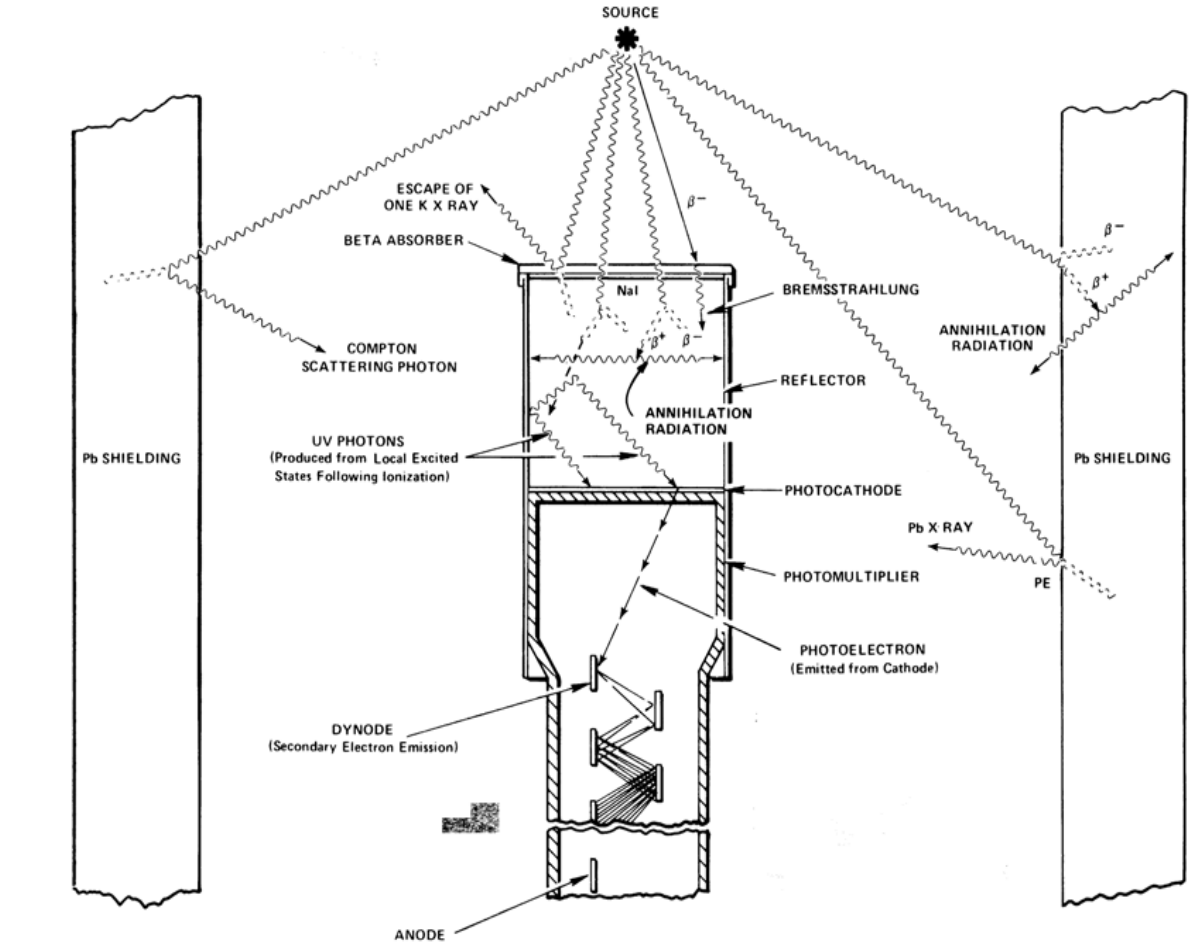

Figure 3.9: Various events in the vicinity of a typical detector (Knoll, 1989).

3.5.2 Detector efficiency

Various kinds of efficiency definitions can be used for gamma ray detectors.

i. Absolute efficiency is the ratio of the number of counts produced by the detector to the number of gamma rays from the source in all directions.

ii. Intrinsic efficiency is the ratio of the number of pulses recorded by the detector to the number of gamma rays striking the detector. This definition is advantageous in that it is not tied to any source-detector geometry hence can be used to compare the performance of different detectors.

iii. Photo peak (Full-energy peak) efficiency is the efficiency for producing full-energy peak pulses only, rather than a pulse efficiency curve of any size of gamma ray. It is dependent of the energy of the photon interacting with it.

iv. Relative efficiency is the full-energy peak efficiency of a detector as compared to that of another detector at a source distance of 25 cm and at 1.33 keV.

Gamma ray spectrometry of NORMS is difficult due to the fact that most gamma ray spectrometers are not able to block background counts due to the radionuclides in the surrounding of the detector. The activity of the sample must therefore be detected on top of all that background in order to obtain a corrected count. Secondly, activity levels in most NORMS is low hence a need for long counting period in order to obtain statistically significant results.

CHAPTER FOUR

MATERIALS AND METHODS

4.1 Materials used in sample collection and analysis

The following materials were used in data collection and analysis.

i. 50 clean 2 kgs capacity polythene papers and labeling stickers.
ii. Garmin (GPS).
iii. Hot air oven.
iv. Plastic bottles, aluminium foil and parking tape.
v. Metallic buckets and 1mm mesh sieve.
vi. 76 mm × 76 mm Thallium activated sodium iodide [NaI(Tl)] detector.
vii. PCA-P software for spectral data acquisition.
viii. Oxford win-MCA and Assayer software version 3.80 for spectral data analysis.
ix. IAEA certified reference samples.

4.2 Sample collection and preparation

22 sand samples were collected around Tharaka region of Tharaka-nithi County. Eight samples (1-8) were collected from Chuka-Igamba Ng'ombe in Kiramankari, Kajuki, Kamutiria, Makomora, Ruguti River, Thuci River, Maara river and Kanthanje. Nine samples (9-17) were collected from Tharaka south in Mutonga River, Ciakariga, Gituma, Makomango and Marimanti. Five samples (18-22) were collected from Tharaka north in Gatue and Kamwathu locations as shown in figure 4.1. To get a representative sample from each sampling site, 0.5 kg of sand was collected in three

locations within an area of about 20 square Ft. and mixed to produce one sample of about 1.5 kg. This would later be reduced to a single sample weighing 300 grams upon crashing and sieving while the rest of the sand was discarded. The exact location for each sampling site was recorded using hand held Garmin GPS (global positioning system model 12). The samples were kept in clean polythene papers and labeled according to the location of the sampling site. The sampling was purposeful depending on the availability and accessibility of sand since the area lacks proper road network, it is thorny and rocky hence making most of the areas inaccessible. Only quality construction sand was considered; during my study I involved the locals in identifying the areas with viable sand as some sand in the area cannot be used for construction purposes due to its poor quality.

The samples were crushed and sieved though 1mm mesh for particle homogeneity then dried in an oven at a temperature of 110 ^{0}C for 22-24 hours to remove moisture. After moisture removal the samples were cooled in a moisture free atmosphere, weighed (300 g) and each stored in sealed plastic bottles. To prevent radon from leakage, the bottle caps were lined with aluminum foil and the caps sealed with a parking tape. The sealed samples and the reference materials were stored for 30 days before counting to allow ^{226}Ra, ^{232}Th and their short-lived decay products to reach secular equilibrium (Mustapha *et al.*, 1999). A gamma ray spectrometer was used to measure the activity of radionuclides in the samples.

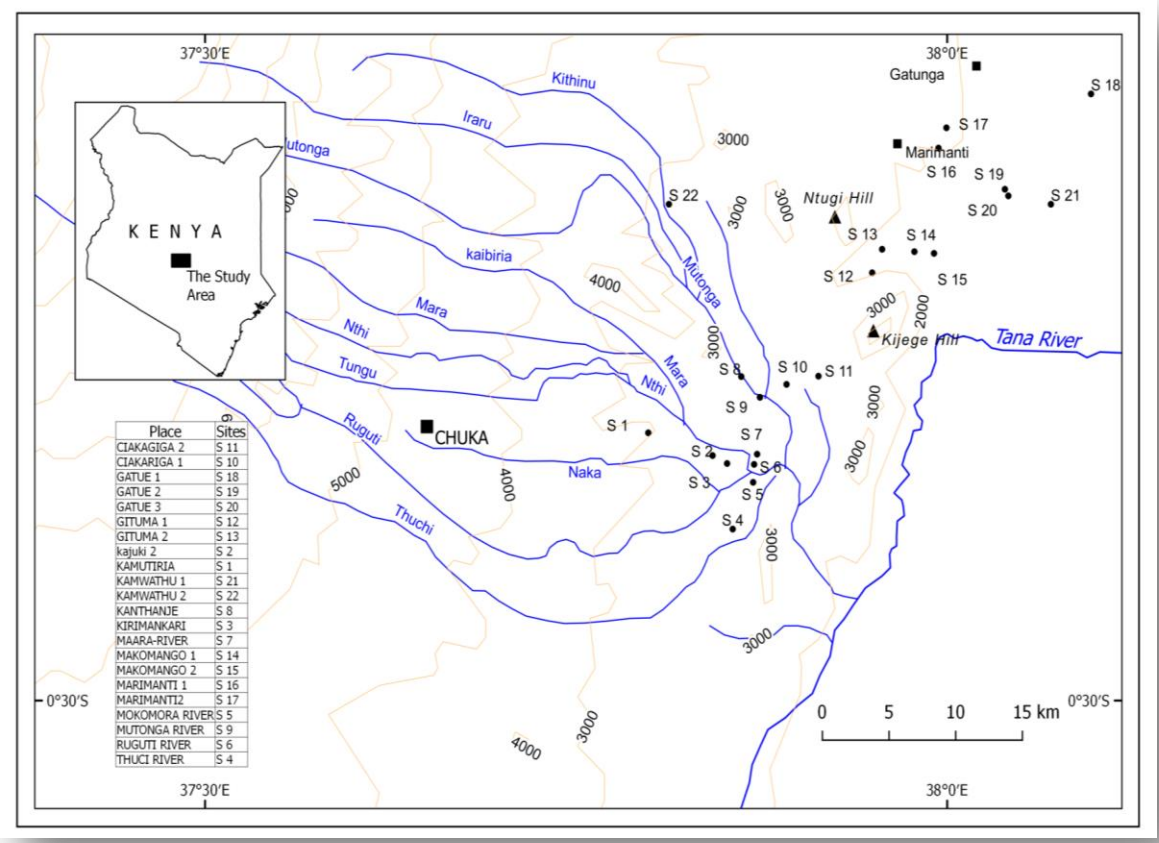

Figure 4.1: A map showing the sampling sites from sand mines in Tharaka Nithi County

4.3 Spectral data acquisition by sodium iodide [NaI (Tl)] detector

Thallium activated sodium iodide [NaI(Tl)] gamma ray spectrometer was used in the identification and quantification of gamma emitting isotopes. The spectrometer consists of a 76 mm ×76 mm NaI(Tl) detector. The system includes an Oxford PCAP multichannel analyzer (MCA) card and its software. The PCAP multichannel analyzer (MCA) consists of a high voltage supply, a charge sensitive pre-amplifier, a shaping amplifier, multichannel analyzer (MCA). The photomultiplier tube converts light from

the detector medium to electric signals. Preamplifier attached to the detector collects the charges produced by the photomultiplier tube and produces a voltage proportional to the input charge (pulses). The amplifier shapes the pulses and increases their sizes.

The multichannel analyzer consists of analogue-to-digital converter (ADC), control logic, memory and display. It rejects out range of pulses from the amplifier; measures height of accepted pulses and adds a count into the memory of location corresponding to the channel representing the voltage range; and displays the data to be saved or printed. Each channel in the detector corresponds to a small range of energies. Each event in the detector produces a voltage proportional to the energy of the gamma ray that caused the event.

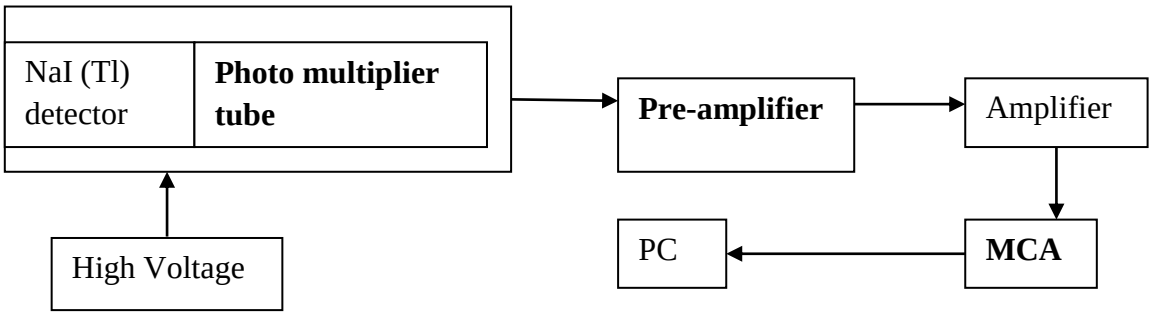

Figure 4.2: Systematic diagram of NaI(Tl) gamma ray spectrometer used in this work

The height of each spectrum is proportional to the number of counts (intensity) and the channel number is proportional to the voltage (energy). The resulting spectrum is thus a plot of intensity versus energy. A systematic diagram of a NaI(Tl) gamma ray spectrometer is as shown in figure 4.2.

4.4 Radioactivity measurements with the spectrometer

The detector was shielded by a thick lead to reduce gamma-ray background. The samples in sealed beakers were placed on the detector and counted for 30000 seconds. This was done for all the samples and also reference samples, maintaining the geometry so as to minimize uncertainties due to measurements (Turhan *et al*, 2008). Maximum effective solid angle for radiation photons hitting the detector is obtained for geometries in which the detector surrounds the source for small volumes or the source surrounds the detector for large volumes (Agora 2012, Debertin and Helmer, 1988). In this study marinelli beakers were used to give maximum distribution for large sample quantity. To prevent backscattered radiation, the inner walls of the shield were not too close to either the source or detector to prevent photons from striking the walls of the shield. A distance of 10 cm is recommended (Agora 2012, Debertin and Hermer, 1988).

4.4.1 Energy calibration of the NaI(Tl) spectrometer

Energy calibration of the detector was done at the start of every measurement to cater for changes in weather vibrations and heating up of the detector. This was to obtain the relationship between peak positions and the corresponding gamma ray energy. This was

achieved by measuring peaks of gamma ray emitting sources of precisely known energy and comparing the measured peak position with energy. In this work,Cs-137 was used to calibrate for photo peaks 662 keV and Co-60 was used to calibrate for photo peaks 1170 keV and 1330 keV; calibration done in the energy range of 350 keV to 3000 keV. The peak positions were measured and the corresponding channel numbers and used to deduce the energy – channel relationship. The peak energies and their corresponding channel numbers were used to plot a second order polynomial function hence producing the corresponding relationship of photon energy as a function of channel number.

The calibration equation of the polynomial fit is given in the form of equation 4.1 as shown below (Debertin and Helmer., 1988; Shikali *et al*., 2014)

$$E = E_O + K_1C + K_2C^2 \qquad (4.1)$$

where E is the photon energy, C is the channel number and (E_0, K_1 and K_2) are fit parameters. The polynomial was generated by using micro cal origin software.

Table 4.1: The fit parameters of the polynomial equation used for energy calibration

Parameter	Fitted value
E_0	-43.100 ± 2.155
K_1	3.92275 ± 0.196
K_2	$-3.0721 \times 10^{-5} \pm 0.154 \times 10^{-5}$

A graphical representation of energy against channel number is as shown below in figure 4.3.

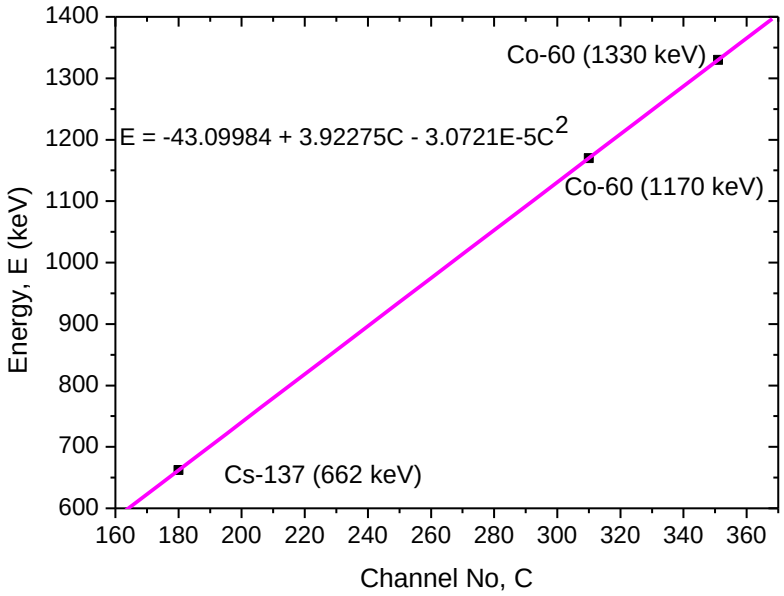

Figure 4.3: Energy calibration of the [NaI (Tl)] detector used. The line represents second order polynomial fit to the data

4.4.2 Determination net intensity in the NaI(Tl) spectrometery

The detector can detect gamma rays from another source outside the sample under analysis. This is referred to as background radiation which can originate from the building materials which house the spectrometer or items in close proximity to the sample under analysis. The background intensity was determined by counting for 300 milliliters of distilled water under the same geometry and acquisition time as the samples with assumption that the water contained no radioactive elements. To obtain the net intensity of a sample, the background intensity was subtracted from the gross

intensity of the sample. The net intensity obtained was then used to calculate activity concentrations as explained in section 4.5.

$$I_n = I_s - I_b \quad (4.2)$$

where I_n is the net intensity of the sample, I_s is the gross intensity of the sample and I_b is the background intensity.

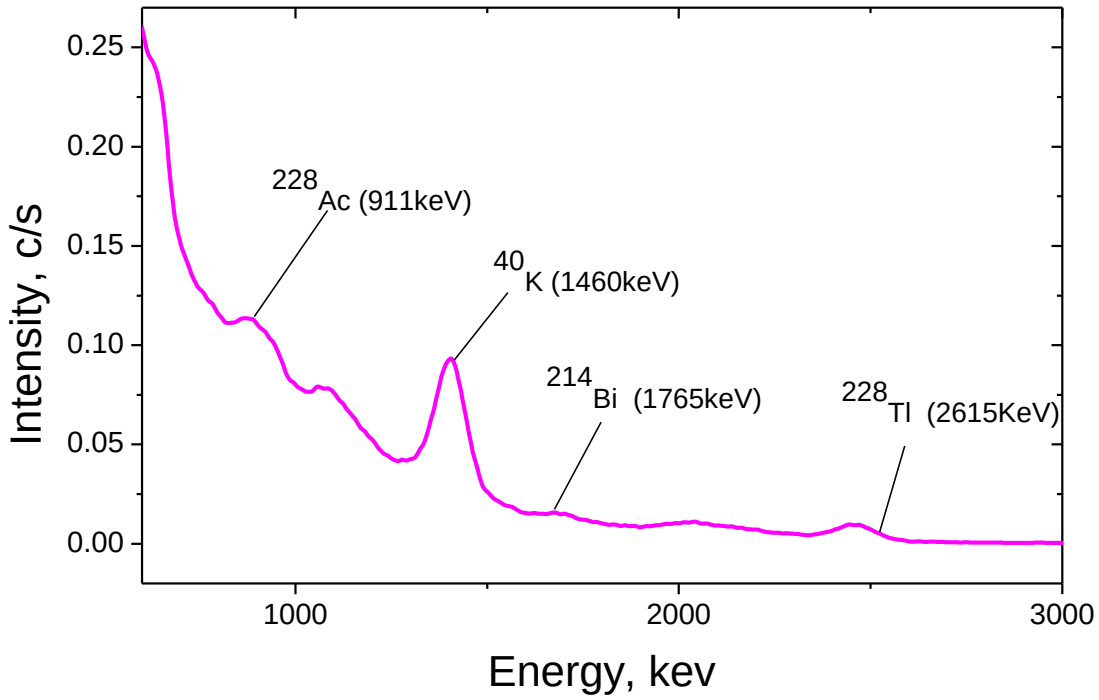

Figure 4.4: A gamma ray spectrum of a sand sample collected at Mutonga river in Tharaka south. The spectral data acquisition time is 30000 seconds

Figures 4.4 is a gamma ray spectrum of sand collected from Mutonga river while figure 4.5 is a gamma ray spectrum of background counts. The peaks of figure 4.4 are slightly

higher than the peaks of figure 4.5 and the difference between the peaks gives the net intensity.

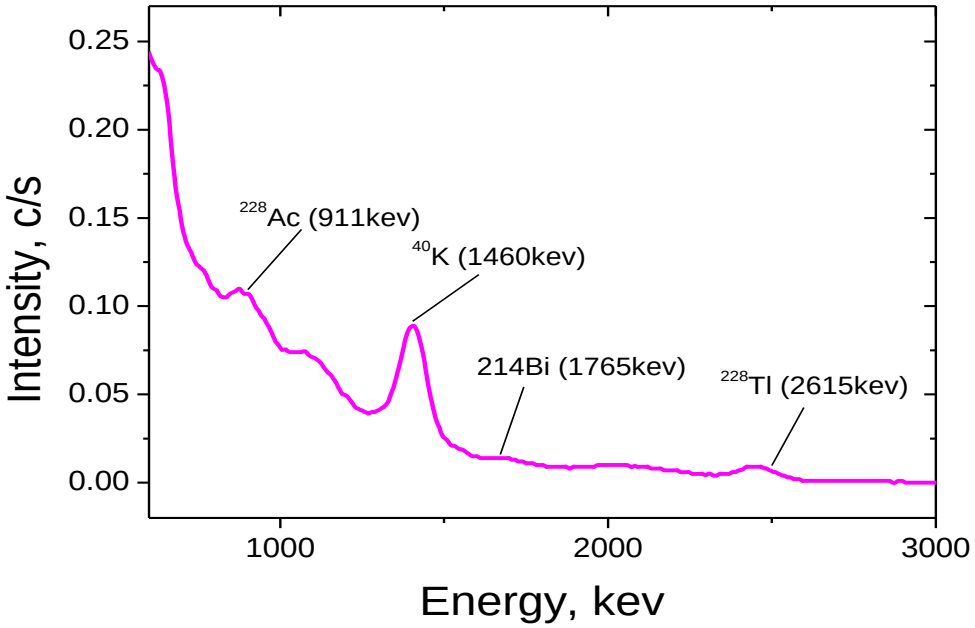

Figure 4.5: Gamma ray spectrum of background counts. The spectral data acquisition time is 30000 seconds

4.4.3 Region of interest in the NaI(Tl) spectrometery

The spectrum of the sample is the sum of composing spectra. In this work the focus was placed in three regions of interest in the determination of gamma activities. The strongly interacting parts of the spectrum were not considered. ^{40}K with peak energy of 1460, ^{214} Bi with a peak energy of 1765 and ^{208}Tl with peak energy of 2615 was chosen to evaluate the intensity of ^{40}K, ^{238}U and ^{232}Th respectively. This is because these peaks weakly interferes with other peaks hence they forming pure peaks of the spectrum.

4.4.4 Detection efficiency of the [NaI(Tl)] spectrometer

The detection efficiency was obtained by use of standard IAEA certified (RGMIX). The activity of the certified samples and the peak counts in respect to the gamma lines 1765 keV for ^{214}Bi, 2615 keV for ^{208}Tl and 1460 keV of ^{40}K was used to calculate efficiency using equation 4.3 (Mustapha, 1999);

$$\varepsilon_i = \frac{n_s - n_b}{ECm_s} \tag{4.3}$$

where ε_i is the counting efficiency of the detector in the energy window corresponding to the radionuclide (i) of interest in RGMIX, n_s is the counting rate recorded in the energy window when the sample holder is filled with the standard material, n_b is the counting rate in the same window when the sample holder is filled with distilled water, E is the photon emission probability, m_s is the mass of the RGMIX standard used and C (Bq/kg) is the activity concentration of a given radionuclide in RGMIX. The gamma lines emission probabilities ρ of the IAEA reference material RGMIX used in equation 4.3 were as follows: ρ = 0.11 at 1460 keV, 0.161 at 1765 keV and 0.36 at 2615 keV (IAEA, 1987). The calculated efficiencies corresponding to the three radionuclides are given in the Table 4.2. The measured efficiency values are in line with values obtained by other researchers (Knoll, 1999); hence the detection efficiency was good.

Table 4.2*:* Efficiencies of emission of ^{40}K, ^{232}Th and ^{238}U in NaI(Tl) spectrometry

Radionuclide of interest	Intensity of radionuclide of interest in RGMIX, I_s (c/s)	Intensity of radionuclide of interest in distilled water, I_b (c/s)	Net intensity, I_s-I_b (c/s)	Emission probability, (ρ)	Concentration (Bq/kg)	Efficiency, (ε) (10^{-3}%)
K-40	1.926	1.066	0.860	0.110	5400	8
U-238	0.057	0.018	0.039	0.161	1260	11
Th-232	0.243	0.115	0.128	0.360	1160	17

4.4.5 Detection limits of the [NaI(Tl)] spectrometer

This is the ability of the detector to record minimum value of the useful signal. This was computed using the relation 4.4 (Mustapha, 1999);

$$l_D = \frac{1}{m_s \varepsilon_i E}\left[\frac{2.71}{T} + 4.65\sqrt{\frac{C_B}{T}}\right. \quad (4.4)$$

where, C_B is the background count rate in the channels of interest and T is the counting time (30000s) of the detector. Other symbols are defined by equation 4.3. The detection limits for ^{40}K, ^{232}Th and ^{226}Ra were found to be 93.5 $BqKg^{-1}$, 40.76 $BqKg^{-1}$ and 33.86 $BqKg^{-1}$ respectively. The detection limits are above the natural background activity concentration levels.

4.4.6 Energy resolution of the detector

Energy resolution of a detector is the ability of a detector to distinguish between two or more closely lying photo peaks, the sharper or narrower the photo peak the greater the resolution. This was done using a Gaussian fitting of cesium-137 photo peak and the fit parameters used to calculate the resolution.

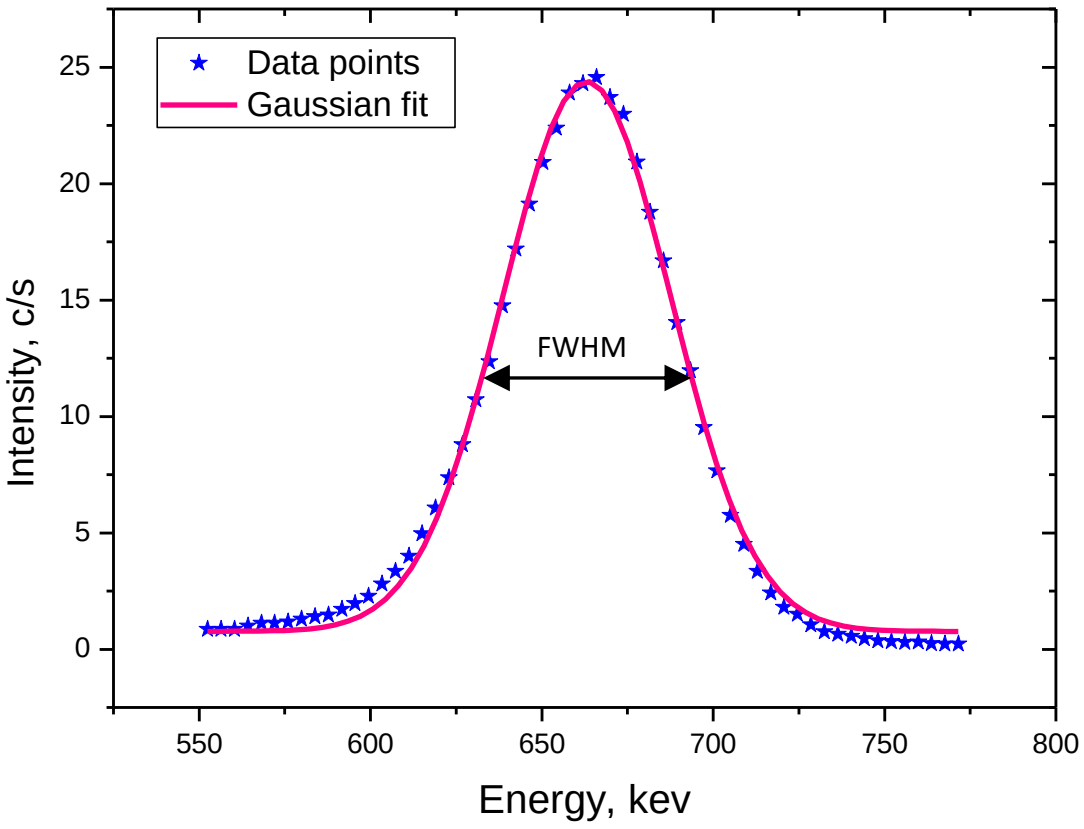

Figure 4.6*:* Gaussian fitting of mono-energetic source cesium-137 used to derive parameters for calculation of energy resolution. This was done after subtraction of the background.

The Gaussian model equation used to generate figure. 4.6 is;

$$y = y_0 + \frac{A}{w\sqrt{\frac{\Pi}{2}}}\exp\left(\frac{-2(x- x_0}{w^2}\right)^2 \quad (4.5)$$

where y_0 is the baseline offset, A is the area under the curve, x_0 is the center of the peak and w is the full width at half maximum. The fit parameters were as shown in table 4.2.

Table 4.3: The parameters generated by Gaussian fit to the peak of cesium-137.

Parameter	Fitted value
Y_0	0.77 ± 0.09 c/s
X_c	663.06 ± 0.20 keV
W	42.22 ± 0.49 keV
A	1457 ± 16 c/s

The chi-square for the fitting was 0.2083.Using the values of full width at half maximum (w) and centroid energy x_c, the resolution (R) of the detector was calculated as;

$$R = \frac{w}{x_c} \times 100\% \quad (4.6)$$

The energy resolution calculated as per equation 4.6 and table 4.2 was found to be 7.4%. The best resolution for 662 keV gamma ray from Cs-137 for a 76mm × 76mm NaI(Tl) detector ranges from 7.5% to 8.5% (Knoll, 1999).

4.5 Calculation of activity concentration

The radioactivity concentration of the radionuclides was calculated after getting the net intensity using comparison method, given by the equation 4.7 as shown below (Mustapha, 1999);

$$\frac{A_s M_s}{I_s} = \frac{A_R M_R}{I_R} \quad (4.7)$$

Where A_s is the radioactivity concentration of radionuclide in the sample, M_s is mass of the sample, I_s is the net peak intensity of the radionuclide in the sample, A_R is the activity concentration of the radionuclide of the reference sample, M_R is the mass of the reference sample and I_R is the net peak intensity of the radionuclide in the reference sample.

4.6 Radium equivalent activity

The distribution of ^{238}U, ^{232}Th and ^{40}K radionuclides is not the same in the environment. Radium equivalent concept allows a single index to be used in describing the gamma output from different mixtures of the above named radionuclides; it was determined by the below equation. (Beretka and Matthew, 1985);

$$Ra_{eq} = A_{Ra} + 1.4286\, A_{Th} + 0.0792\, A_k \quad (4.8)$$

where 1, 1.4286 and 0.07692 are conversion constants for Uranium, Thorium and

Potassium respectively and A_{Ra}, A_{Th}, and A_K are activity concentrations of activity concentrations in Bq/kg respectively. Radium equivalent represents a weighted sum of activities of ^{238}U, ^{232}Th and ^{40}K and is based on the assumption that 370 Bq/kg of ^{238}U, 259 Bq/kg of ^{232}Th, 4810 Bq/kg of ^{40}K produce the same gamma ray dose (Otwoma *et al*, 2013).The index is used to assess the suitability of a material for building and the maximum value of Ra_{eq} in building materials and products should be less than 370 Bq/kg for safe use.

4.7 Radiation hazard indices

4.7.1 External hazard index

This is due to external exposure to excess gamma radiation from the natural radionuclides in the construction building materials. It was calculated with the assumption that 370 Bq/kg of ^{238}U, 259 Bq/kg of ^{232}Th, 4810 Bq/kg of ^{40}K produce the same gamma ray dose and limiting the external gamma radiation up to 1.5 msv/y. The external hazard index is denoted by H_{ex} was calculated using the equation 4.9 (Shoeib and Thabayneh 2014).

$$H_{ex} = \frac{A_{Ra}}{370} + \frac{A_{Th}}{259} + \frac{A_k}{4810} \qquad (4.9)$$

The value of this index must be less than unity to keep the radiation risks negligible. The maximum acceptable value of H_{ex} of unity corresponds to the upper limit of radium activity (370 Bq/kg) and permissible dose equivalent limit of 1 msv/y.

4.7.2 Internal hazard index

Short lived radon and it's daughter products are internally hazardous to the respiratory organs. The internal exposure to radon and it's progenies is referred to as internal hazard index denoted by H_{in}. It was given by the equation 4.10 (Shoeib and Thabayneh, 2014);

$$H_{in} = \frac{A_{Ra}}{185} + \frac{A_{Th}}{259} + \frac{A_k}{4810} \qquad (4.10)$$

If the maximum concentration of ^{226}Ra is half than that of the normal acceptable limit, then H_{in} will be less than unit (Kinsara *et al.,* 2014). The value of this index should be less than unit in order for the radiation hazard to have negligible hazardous effects of radon to the respiratory organs of the public (Beretka and Mathew, 1985).

4.8 Absorbed dose rates

Absorbed dose rates can be classified as either indoor or outdoor. Indoor dose rate is experienced inside a room and it depends on the type of the house and also the construction materials used. Building materials from high background radiation areas have high levels of indoor absorbed dose rates. Outdoor dose rate is experienced outside the room; it is mainly experienced by miners who spend a lot of time harvesting the sand.

4.8.1 Outdoor gamma radiation dose rate

The activity concentrations in Bq/kg of ^{238}U, ^{232}Th and ^{40}K were used to calculate outdoor absorbed dose rates due to terrestrial gamma rays 1m above the ground. This was given by the below equation (Abbady *et al*., 2005; Agora 2012);

$$D_o = 0.0417A_K + 0.462A_{Ra} + 0.604A_{Th} \quad (4.11)$$

where 0.0417 $nGyh^{-1}/Bqkg^{-1}$, 0.462 $nGyh^{-1}/Bqkg^{-1}$ and 0.604 $nGyh^{-1}/Bqkg^{-1}$ are dose conversion factors coefficients of ^{40}K, ^{238}U and ^{232}Th respectively (UNSCEAR, 2008). The world average outdoor terrestrial gamma ray exposure rate is 54 nGy/h (UNSCEAR, 2008).

4.8.2 Indoor gamma ray radiation dose rate

The indoor absorbed gamma ray radiation dose rate was calculated using EC, 112 (1999) guidelines using equation 4.12;

$$D_i = 0.057A_K + 0.67A_{Ra} + 0.78A_{Th} \quad (4.12)$$

where 0.057, 0.67 and 0.78 are specific dose rates in $nGyh^{-1}/Bqkg^{-1}$ of ^{40}K, ^{238}U and ^{232}Th respectively (EC, 1998). The parameter values used in calculating doses are based on the model room of dimensions 4m × 5m × 2.8m (EC, 1998), and were determined by Monte Carlo simulation. The model house is one which the floors and walls are made of concrete that contain the sand while the ceiling is made of wooden or plastic materials

typical to the building constructed using sand from Tharaka region. In determination of conversion coefficients, it is assumed that all decay products of ^{238}U, ^{232}Th are in radioactive equilibrium. The concrete structure shield's the house against gamma radiation from the undisturbed earth's crust. The world's average value of background radiation is 60 $nGyh^{-1}$ (UNSCEAR 2000). The excess dose rate was calculated by subtracting the background from the calculated indoor dose rate. The worldwide average indoor absorbed dose rate in air is 84 $nGyh^{-1}$ (UNSCEAR, 2008).

4.9 Annual effective dose rate

To estimate annual effective doses, one must take into account the conversion coefficients from the absorbed dose in air to effective dose and indoor occupancy factor. The average numerical values for those parameters vary with the age of the population and the climate of the location (UNSCEAR 2000). In the Tharaka Nithi County, children who form a big part of the total population spend most of the times at homes and at school in classrooms. Majority of the working population spend approximately twelve hours per day on weekdays and more time on weekends indoors. This translates into an average about fourteen hours per day indoors hence occupancy factors of 0.6 and 0.4 were applied for indoor and outdoor respectively (Mustapha *et al*., 1997). In this study the value of conversion factor from absorbed dose in air to effective dose received by human beings applied that used was 0.7 Svy^{-1} (UNSCEAR, 2008). The indoor annual effective dose rate is experienced by the house dwellers who live in the houses constructed using the sand while outdoor annual effective dose rate is for the miners

who spend most of the times mining and loading the sand to the lorries.

The outdoor and indoor annual effective dose rates in $mSvy^{-1}$ were calculated using equation 4.13 (UNSEAR, 2000);

$$E = D \times T \times Q \times 10^{-6} \quad (4.13)$$

Where D is the absorbed dose rate in $nGyh^{-1}$, T is the occupancy time and Q is the conversion factor. The indoor occupancy factor used was 0.6 while outdoor occupancy factor was 0.4. The outdoor and indoor absorbed dose rates used in calculation of annual effective dose rates were calculated as per equation 4.9 and 4.10 respectively.

CHAPTER FIVE

RESULTS AND DISCUSSIONS

5.1 Introduction

Gamma ray spectrometric analysis of construction sand from Tharaka region of Tharaka Nithi County has been done. The activity concentrations, hazard indices and dose rates have been calculated and their values compared with recommended limits to assess if the sand can be used for construction without causing any danger to human beings (ICRP, 1993; ICRP, 2000). The results have also been compared with the world averages and results from other regions where similar researches have been done.

5.2 Radioactivity concentration of natural radionuclides in the building sand.

The activity concentrations in the samples were calculated in $Bqkg^{-1}$ using a method of comparison and the results tabulated in table 5.1. They ranged from 32 $Bqkg^{-1}$ to 2662 $Bqkg^{-1}$ with an average value of 1069 ± 46 $Bqkg^{-1}$ for ^{40}K, 19 $Bqkg^{-1}$ to 269 $Bqkg^{-1}$ with a mean of 96 ± 4 $Bqkg^{-1}$ for ^{238}U and 11 $Bqkg^{-1}$ to 114 $Bqkg^{-1}$ with an average of 53 ± 3 $Bqkg^{-1}$for ^{232}Th as shown on figure 5.1. The results indicate a great variation in the mean activity concentrations of the analyzed naturally occurring radionuclides (^{40}K, ^{238}U and ^{232}Th) in the samples. The variation in the activity concentrations in the sample varied with the sample location due to geological formation and the level of soil erosion in the place.

Table 5.1: Activity concentration of ^{40}K, ^{238}U and ^{232}Th (Bq/kg) in the sand samples.

SITE	LOCATION	^{40}K	^{238}U	^{232}Th
Sample 1	KAMUTIRIA	452 ± 21	135 ± 7	33 ± 3
Sample 2	KAJUKI	1226 ± 43	77 ± 3	11 ± 1
Sample 3	KIRIMANKARI	1323 ± 56	38 ± 2	87 ± 5
Sample 4	THUCI RIVER	887 ± 32	77 ± 3	76 ± 5
Sample 5	MOKOMORA	97 ± 8	19 ± 1	16 ± 1
Sample 6	RUGUTI RIVER	32 ± 2	77 ± 4	44 ± 3
Sample 7	MAARA-RIVER	1388 ± 58	38 ± 2	98 ± 2
Sample 8	KANTHANJE	2146 ± 100	77 ± 3	65 ± 4
Sample 9	MUTONGA RIVER	920 ± 35	192 ± 8	87 ± 5
Sample 10	CIAKARIGA 1	436 ± 20	173 ± 9	54 ± 4
Sample 11	CIAKAGIGA 2	516 ± 23	96 ± 5	49 ± 3
Sample 12	GITUMA 1	1420 ± 65	173 ± 9	87 ± 6
Sample 13	GITUMA 2	1646 ± 81	96 ± 5	44 ± 3
Sample 14	MAKOMANGO 1	307 ± 14	269 ± 13	60 ± 4
Sample 15	MAKOMANGO 2	452 ± 21	135 ± 7	33 ± 2
Sample 16	MARIMANTI 1	2259 ± 90	212 ± 8	49 ± 3
Sample 17	MARIMANTI 2	936 ± 42	19 ± 1	32 ±2
Sample 18	GATUE 1	194 ± 8	58 ± 2	22 ± 1
Sample 19	GATUE 2	1291 ± 57	19 ± 1	16 ± 1
Sample 20	GATUE 3	2259 ± 96	96 ± 5	114 ± 7
Sample 21	KAMWATHU 1	662 ± 28	19 ± 1	38 ± 2
Sample 22	KAMWATHU 2	2662 ± 122	19 ± 1	49 ± 3
MEAN VALUES		**1069 ± 46**	**96 ± 4**	**53 ± 3**

Most of the samples were collected along the gullies due to the massive soil erosion that

characterize the place while a few samples were collected along river banks. Generally the average activity concentration of potassium was found to be more than double the world average of 420 Bq/kg, while that of ^{238}U was found to be triple the world average of 33 Bq/kg as shown on figure 5.1.

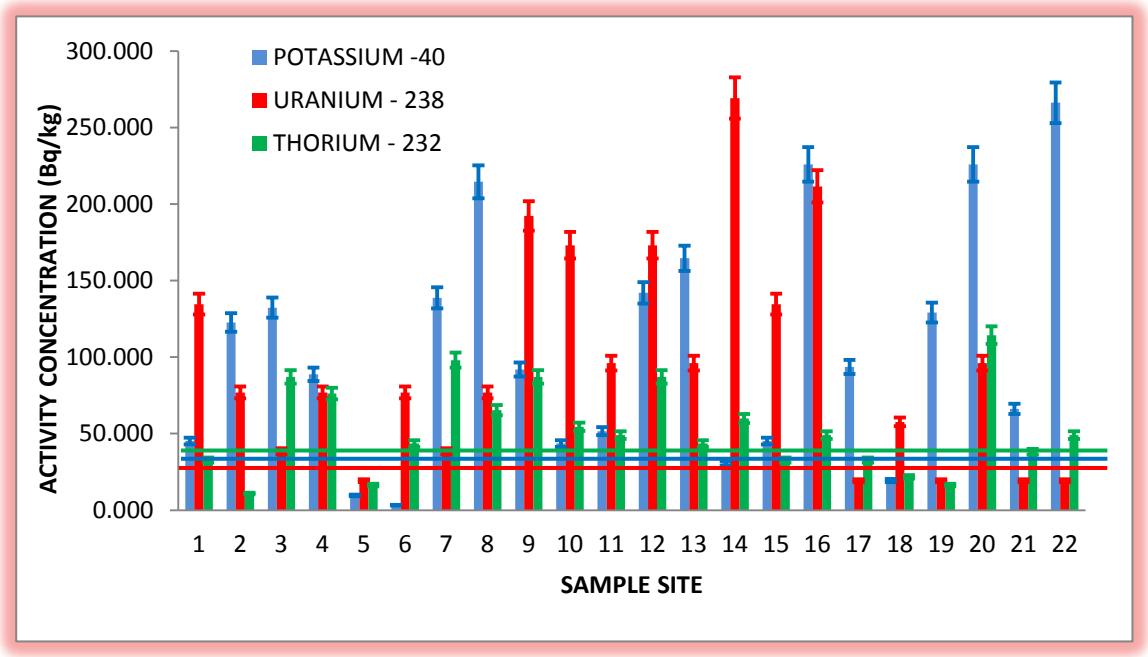

Figure 5.1: Comparison of the activity concentration of ^{40}K, ^{238}U and ^{232}Th in the samples. The activity concentration of potassium has been reduced by a factor of ten for clarity of ^{238}U and ^{232}Th.The lines show how the values compare with world averages of 420, 33 and 45 $Bqkg^{-1}$ for ^{40}K, ^{238}U and ^{232}Th respectively.

Generally, activity concentration of potassium was high in most of the samples apart from four samples picked from sampling sites 5, 6, 14 and 18 which recorded the values below world average as shown on figure 5.1. The sand mined in the area has been observed to have high silica content (Schoeman, 1951); the high concentration of

potassium is attributed to the formation of silicate (SiO_2) during cooling and solidification of igneous rocks since the region forms the basement of Mount Kenya. This is in agreement with the study of Schoeman (1951) who reported most rocks with elevated levels of potassium feldspar in the region.Potassium is highly compatible with silica than Thorium and Uranium hence it was abundant most in the region (Adel and E-Taler, 2005; Agora, 2012).

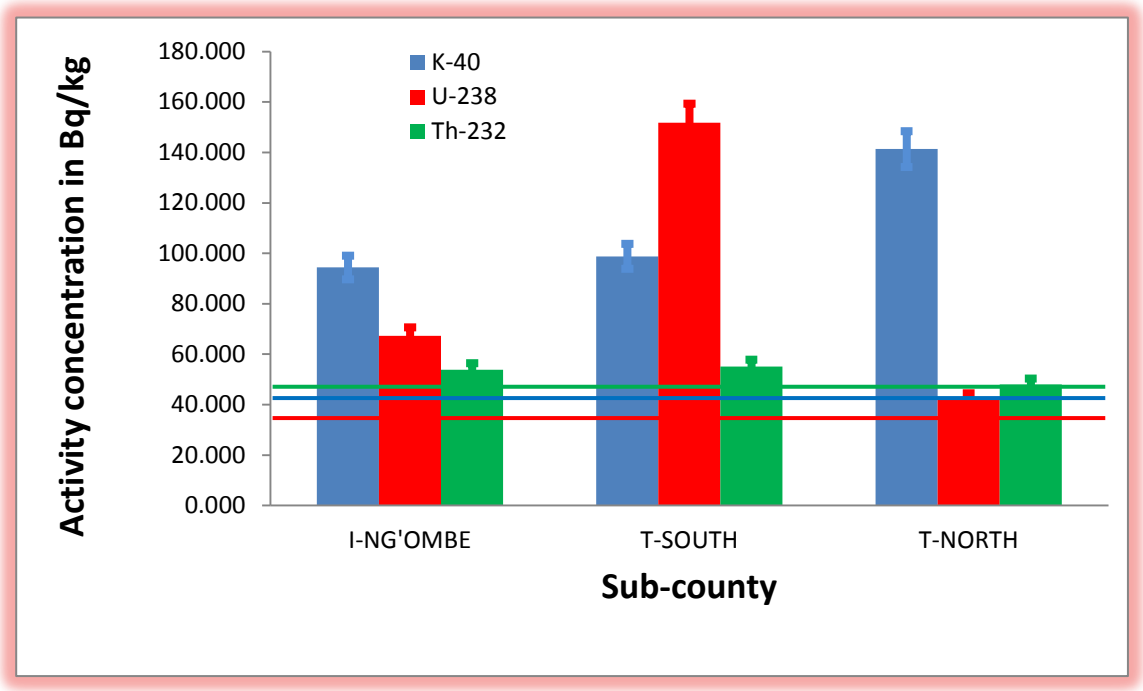

Figure 5.2: Comparison of activity concentrations of ^{40}K, ^{238}U and ^{232}Th in the three sub-counties. The activity concentration of potassium has been reduced by a factor of ten for clarity of $^{238}U$and ^{232}Th. The lines show how the values compare with world averages of 420, 33 and 45 $Bqkg^{-1}$ for ^{40}K, ^{238}U and ^{232}Th respectively.

Sample collected from sample site 5 recorded the lowest activity concentrations of the

three radionuclides; this is due to heavy presence of Gabbro in the region which is associated with no radioactivity. Tharaka south recorded the highest average values of activity concentration of uranium with 152 ± 7 Bq/kg while Igamba Ng'ombe and Tharaka north recorded 67 ± 3 Bq/kg and 42 ± 2 Bq/kg respectively as shown on figure 5.2. The average activity concentrations of Thorium in all the sub-counties were within the same range with Tharaka-south, Igamba Ng'ombe and Tharaka north recording 55 ± 4, 54 ± 3 and 48 ± 3 respectively. The average activity concentration of ^{238}U in Tharaka south is about five times the world average of 33 Bq/kg as shown in figure 5.2. Uranium is present as trace amount in major minerals such as quartz and feldspar, its mode of occurrence is through the following possibilities; isomorphous substitution in the lattice, concentration in the lattice defects, adsorption along crystal imperfection and grain borders and lastly inclusion as microcrystal of uranium minerals (IAEA, 2009). High adsorption is associated with organic matter, iron and manganese oxides. Goethite, hematite and ferrihydrite present on the surfaces of iron nodules scavenge uranium from ground water. Aging of the surface oxides results in the stabilization of adsorbed uranium. There is presence of iron oxide in Tharaka region (Schoeman, 1951); The high levels of average activity concentration of uranium in Tharaka south is attributed by the presence of iron oxide which plays an important role in controlling the retention and distribution of uranium (IAEA, 2009).

Although the activity concentration of thorium is low it is uniformly distributed within the region with only a few extreme values. Uranium on the other hand is poorly distributed in the region with some areas recording very high values and others very low

values of activity concentration. The difference in the uranium and thorium contents in the samples may be due to the large differences in the mobility of the two elements. Thorium is much less mobile than uranium. Uranium is a mobile element and tends to accumulate in the late differentiates of igneous melts, primarily because the uranium U^{+4} has a high charge which prevents it from substituting any other element its own size. Uranium is predominantly found in the U^{+4} and U^{+6} oxidation states in the environment; U^{+6} is more soluble and mobile than U^{+4} (IAEA,2009). Semiarid conditions in the area also aid preservation of uranium near the surface. The highest value of uranium content was registered at Makomango in Tharaka south, on the foot of Kijege hills. These are believed to have been deposited at the foot of the hill by soil erosion.

Regression plots of figure 5.3 shows correlation between activity concentrations of ^{232}Th and ^{238}U in the sand samples. The regression plot indicates that there is so much diversity in terms of distribution of thorium and uranium in the region. This could be due to difference in the types of rocks from which the sand originated from and also the difference in solubility of the two.

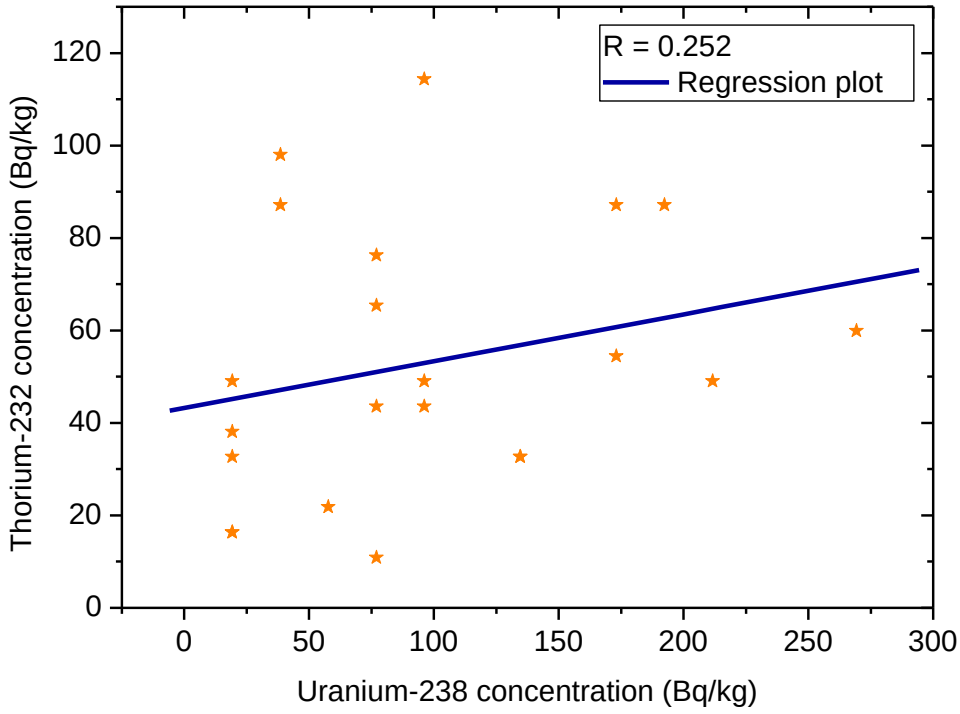

Figure 5.3: Regression plot showing correlation between activity concentrations of ^{232}Th and ^{238}U

Figure 5.4. is a scatter plot ^{238}U/^{232}Th activity concentration ratio; it shows that apart from six samples collected from sampling sites 3, 7, 17, 20, 21, and 22, all other samples contain higher activity concentration of ^{238}U than ^{232}Th. This is attributed to the geological outline of the area. While the presence of Uranium is associated with adsorption by iron oxide, Thorium is not compatible with the chemical components in the schist, psammitic rock, migmatites and intrusives rocks found in the region. Thorium is normally found in elevated amounts in most carbonatite and monazite rocks; which are not characteristic in the region of study (Achola, 2009).

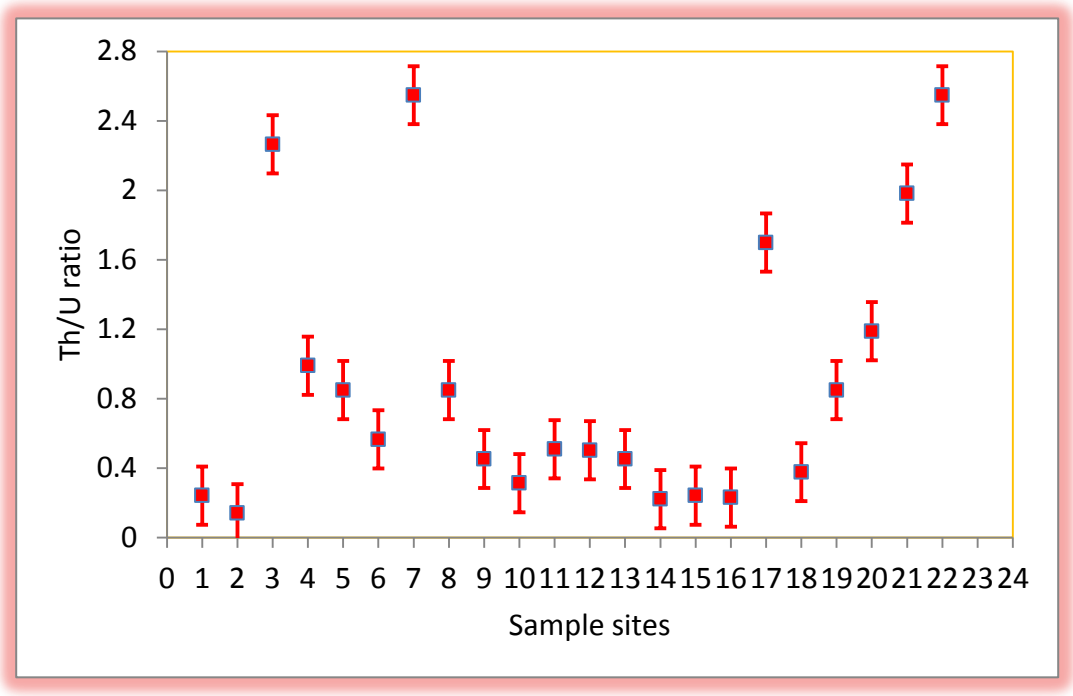

Figure 5.4: A scatter plot of uranium versus thorium ratio in the sand samples**.**

The results of mean activity concentrations in construction sand obtained in this work are compared with results reported in other parts of Kenya and around the world in table 5.2. In the table, the regions recording high levels of activity concentrations have presence of radioactive rich igneous rock, monazites, carbonatite rocks and farming activities where fertilizer introduces potassium and uranium in the soil. From the table, the results obtained compared well with those obtained in other parts of the world.

Table 5.2: Comparison of the average activity concentrations of radionuclides in construction sands in the current study to other parts of Kenya and around the world.

Country	**^{40}K (Bqkg^{-1})**	**^{238}U (Bqkg-^{1})**	**^{232}Th (Bqkg^{-1})**	**References**
Kenya	1068 ± 46	96 ± 4	53 ± 3	This work
Kenya	756 ± 36	128 ± 8	98 ± 6	Shikali et al., 2014 (Kakamega)
Kenya	802	11	5	Mustapha et al., 1999 (Machakos)
Saudi Arabia	139	29	158	Kinsara et al., 2014 (Hail province)
India	777.0 ±7.9	63.5±3.8	89.5±2.5	Gupta et al.,2010
Nigeria	276.42±67.90	28.08±6.99	22.73±9.87	Ajayi et al., 2013 (Ogbomoso)
China	891	23	36	Xinwei and Xiaolan, 2008 (Baoji, west china)

5.3 Statistical analysis of activity concentrations of radionuclide in the sand samples.

The statistical analysis of the activity concentrations of ^{40}K, ^{238}U and ^{232}Th in all the sand samples were done and the results summarized on table 5.3. ^{40}K and ^{232}Th indicate asymmetrical distribution with the tail extending towards high concentration (positive skewness) while ^{238}U has negative skewness. From table 5.3, the measured activity concentration of the three radionuclides shows a strong evidence of normal distribution given that the values for kurtosis and skewness are within the range of normal distribution for the measured samples (http://www.tc3.edu/instruct). All the three radionuclides recorded a high value of standard deviation implying that there are no regular trends in variation of radioactivity in the radionuclides for the construction sand

in the study area. This indicates a strong adversity of sand in the area due to non-uniformity in chemical and geochemical properties in the sand.

Table 5.3: Statistical summary of the activity concentration of radionuclide in the sand samples analyzed in this work.

	No of samples	Min value	Max value	Mean	Skewness	Kurtosis	Std. Dev
^{40}K	22	32.270	2662.35	1068.61	0.528	-0.747	747.75
^{238}U	22	19.240	269.310	98.180	-0.707	-0.309	69.630
^{232}Th	22	10.890	114.370	52.980	0.467	-0.682	27.920

5.4 Radiation hazard indices

Due to non-uniformity in the distribution of radionuclides ^{40}K, ^{238}U and ^{232}Th in the region, Ra_{eq} was introduced. Exposure to gamma radiation originating from construction sand in the region was calculated in terms of radium equivalent and the results tabulated in Table 5.4. The values ranged from 50.24 $Bqkg^{-1}$ in sand samples collected from sample site 5 to 460.83 $Bqkg^{-1}$ in sand samples collected from sample site 16 with a mean value of 256.50 ± 13.04 $Bqkg^{-1}$. A scatter plot of radium equivalent is shown in Fig 5.5. It indicates that only five samples in the area of study recorded the values above the recommended limit of 370 Bq/kg with Tharaka-south having four of the samples. This is due to high levels of activity concentrations of ^{238}U in the samples collected in the region as shown in Fig 5.2. The values of external hazard indices in the sand samples were calculated as shown in Table 5.4. They ranged from 0.14 to 1.23 with a mean of 0.69 ± 0.03. The mean value was below the recommended limit of unity making the sand in the area safe for construction without posing any significant health

effects to the general public according to European Commission on radiation protection (1999). Internal hazard indices associated with the sand samples were also calculated as shown in table 5.4. Their values ranged from 0.19 to 1.80 with a mean value of 0.95 ± 0.05. For safe use of materials for construction H_{in} should be less than unity according (ICRP, 2000).

Table 5.4: The hazard indices of the sand samples collected from Tharaka Nithi County.

Site	Ra_{eq}	H_{ex}	H_{in}
Sample 1	217 ± 12	0.58 ± 0.03	0.95 ± 0.04
Sample 2	190 ± 7	0.50 ± 0.02	0.71 ± 0.02
Sample 3	268 ± 13	0.72 ± 0.03	0.82 ± 0.04
Sample 4	256 ± 12	0.69 ± 0.03	0.89 ± 0.04
Sample 5	50 ± 3	0.14 ± 0.01	0.19 ± 0.02
Sample 6	142 ± 9	0.38 ± 0.02	0.59 ± 0.03
Sample 7	288 ± 15	0.77 ± 0.04	0.87 ± 0.05
Sample 8	340 ± 18	0.91 ± 0.05	1.11 ± 0.07
Sample 9	390 ± 18	1.05 ± 0.05	1.57 ± 0.07
Sample 10	285 ± 16	0.77 ± 0.04	1.24 ± 0.05
Sample 11	207 ± 11	0.56 ± 0.03	0.82 ± 0.05
Sample 12	410 ± 22	1.10 ± 0.06	1.57 ± 0.07
Sample 13	289 ± 16	0.77 ± 0.04	1.03 ± 0.08
Sample 14	379 ± 20	1.02 ± 0.05	1.75 ± 0.07
Sample 15	217 ± 12	0.58 ± 0.03	0.95 ± 0.05
Sample 16	461 ± 20	1.23 ± 0.05	1.80 ± 0.06
Sample 17	140 ± 7	0.37 ± 0.02	0.42 ± 0.03
Sample 18	104 ± 5	0.28 ± 0.01	0.44 ± 0.02
Sample 19	145 ± 7	0.38 ± 0.02	0.44 ± 0.03
Sample 20	438 ± 23	1.17 ± 0.06	1.43 ± 0.06
Sample 21	126 ± 7	0.34 ± 0.02	0.39 ± 0.02
Sample 22	300 ± 15	0.79 ± 0.04	0.85 ± 0.04
Minimum	50 ± 3	0.14 ± 0.01	0.19 ± 0.02
Maximum	461 ± 20	1.23 ± 0.05	1.80 ± 0.06
Samples average	**257 ± 13**	**0.69 ± 0.03**	**0.95 ± 0.05**

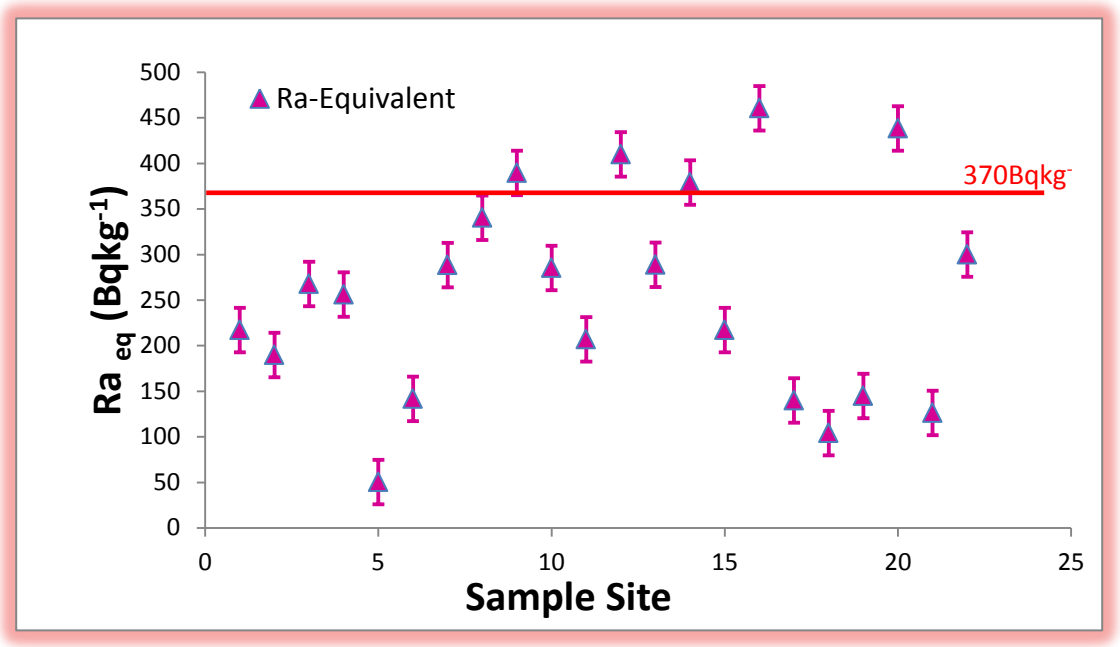

Figure 5.5: A plot scatter of radium equivalent activity in the sand samples. The recommended limit is 370Bqkg^{-1}(ICRP, 2000).

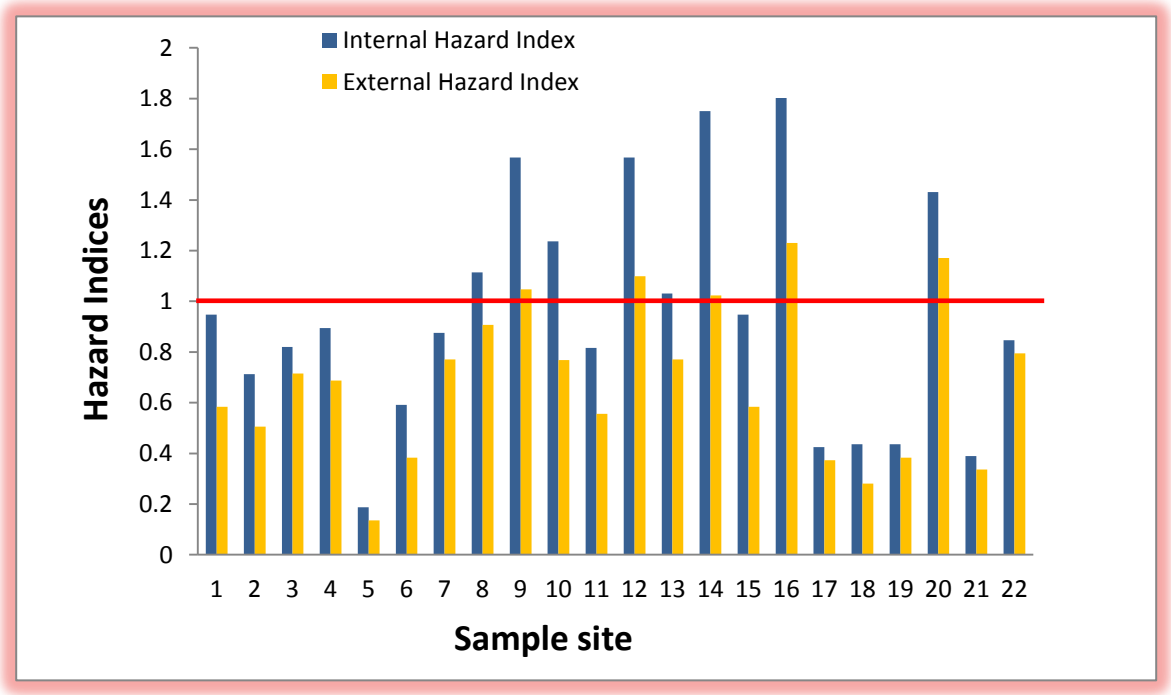

Figure 5.6*:* A plot of internal hazard indices and external hazard indices for the sand samples. The recommended limit is unity (ICRP, 2000).

A bar graph of external hazard indices and internal hazard indices in figure 5.6 indicates that samples of sand from sample sites 9, 12, 14 and 16 all from Tharaka south recorded the highest values of H_{in}, which was above the recommended limit. This is because of high uranium levels in the region as indicated in figure 5.2. The hazard indices associated with construction sand in this region are compared with hazard indices of construction sand reported in other regions in table 5.5.

Table 5.5: Radium equivalent, external hazard index and internal hazard index obtained in this study as compared to the values obtained in other countries.

Country	Ra_{eq}	H_{ex}	Hin	Reference
Kenya	256.50	0.69	0.95	This work
Kenya	321.87	0.883	-	Shikali, 2013, Kakamega
Saudi arabia	265	0.7	0.8	Kinsara *et al*., 2014 (Hail province)
Nigeria	81.82	0.22	0.29	Ayaji *et al*., 2013 (Ogbomoso)
India	251	-	-	Gupta *et al.*, 2010

5.5: Absorbed dose rate and annual effective dose rates.

The values of outdoor dose rates in the samples were calculated and found to vary from between 22.79 $nGyh^{-1}$ to 221.56 $nGyh^{-1}$ with a mean of 120.99 ± 6.07 $nGyh^{-1}$. Indoor absorbed dose rate for the sand samples were higher than outdoor dose rates for all the samples and varied from 31.15 $nGyh^{-1}$ to 308.77 $nGyh^{-1}$ with a mean value of 166.67 $nGyh^{-1}$. The plot in figure 5.5 shows that these mean values are twice the world average

of 54.00 $nGyh^{-1}$ and 84 $nGyh^{-1}$ for outdoor and indoor respectively (UNSCEAR, 2008).

Table 5.6: Absorbed dose rates and annual effective dose rate obtained in this study, the initials B/Bg have been used to mean below background for the neatness of the table.

Site	D_i ($nGyh^{-1}$)	Excess D_i ($nGyh^{-1}$)	D_o ($nGyh^{-1}$)	E_i ($mSvy^{-1}$)	Excess E_i ($mSvy^{-1}$)	Eo ($mSvy^{-1}$)
Sample 1	141	81	101	0.52	0.30	0.25
Sample 2	130	70	93	0.48	0.26	0.23
Sample 3	169	109	126	0.62	0.40	0.31
Sample 4	162	101	119	0.60	0.37	0.29
Sample 5	31	B/Bg	23	0.15	B/Bg	0.06
Sample 6	87	27	63	0.32	0.10	0.16
Sample 7	181	121	135	0.67	0.45	0.33
Sample 8	225	164	165	0.83	0.61	0.40
Sample 9	249	189	180	0.93	0.70	0.44
Sample 10	183	123	131	0.67	0.45	0.32
Sample11	132	72	96	0.49	0.27	0.23
Sample 12	265	205	192	0.98	0.75	0.47
Sample 13	192	132	139	0.71	0.48	0.34
Sample 14	245	15	173	0.90	0.68	0.43
Sample 15	141	81	101	0.52	0.30	0.25
Sample 16	309	249	222	1.14	0.92	0.54
Sample 17	92	32	68	0.34	0.12	0.17
Sample 18	67	7	48	0.25	0.03	0.12
Sample 19	99	39	73	0.37	0.14	0.18
Sample 20	282	222	208	1.04	0.82	0.51
Sample 21	80	20	60	0.30	0.08	0.15
Sample 22	203	143	150	0.75	0.53	0.37
Mean	**167**	**108**	**121**	**0.61**	**0.40**	**0.30**

In all samples the annual effective dose rates due to indoor exposure are greater than outdoor annual effective dose rates as recorded in table 5.6. This is as a result of high indoor absorbed dose rate observed in all the sand samples. The computed values of

annual effective dose rates varied from 0.115 $mSvy^{-1}$ to 1.136 $mSvy^{-1}$ with a mean of 0.613 ± 0.061 $mSvy^{-1}$ and 0.056 $mSvy^{-1}$ to 0.5435 $mSvy^{-1}$ with a mean of 0.297$mSvy^{-1}$ for indoor and outdoor respectively. The average values for both indoor and outdoor annual effective dose rates were higher than world averages of 0.41 $msvy^{-1}$ and 0.07 $mSvy^{-1}$ respectively (UNSCEAR, 2008).

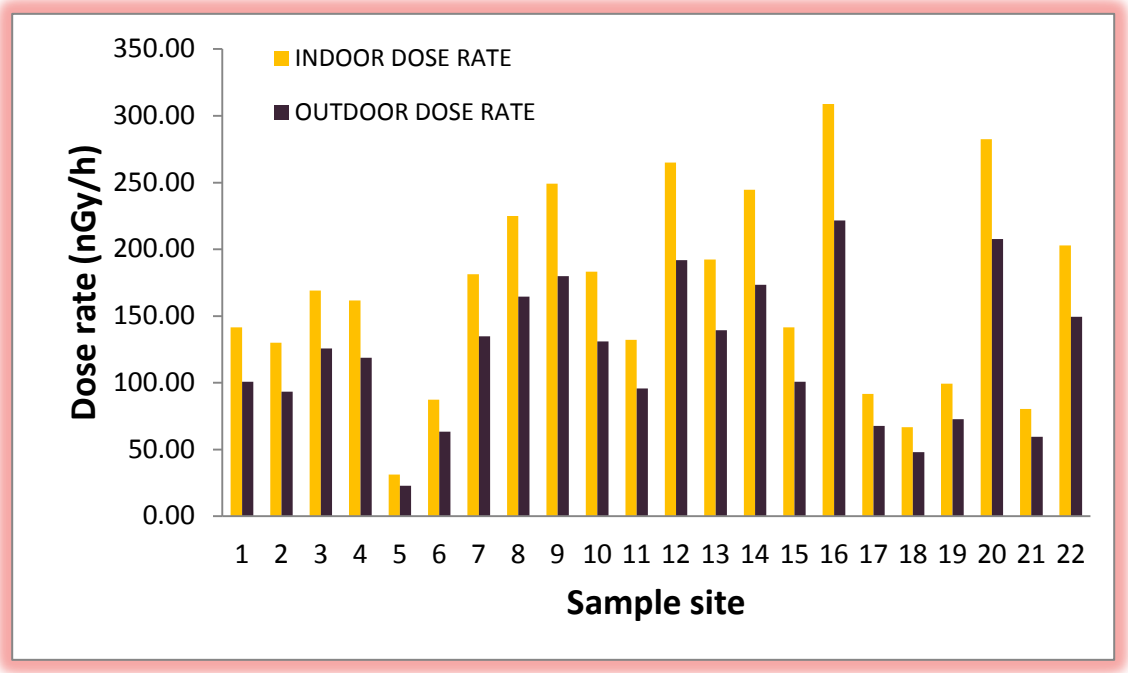

Figure 5.7: Comparison between indoor and outdoor annual effective dose rates for all the sand samples.

Sand collected from Sample site 5 had the lowest dose rates due to low activity concentration of ^{40}K, ^{238}U and ^{232}Th in the sample while those collected from sample site 16 recorded the highest dose rates; this was attributed to high activity concentration levels of ^{40}K and ^{238}U in the sample as recorded in Table 5.1. Using the guidelines in section 4.8, the excess indoor absorbed dose rates and excess indoor annual effective

dose rates were calculated and found to have mean values of 107.985 ± 8.313 $nGyh^{-1}$ and 0.397 ± 0.061 $mSvy^{-1}$ respectively. The world average absorbed dose rate from terrestrial gamma radiation is 60 $nGyh^{-1}$ (UNSCEAR 2000), sample five recorded a value that was below the background value hence excess indoor annual effective dose rate for the sample was also below the background value. With occupational time of 40% outdoor and 60 % indoor, the indoor background annual effective dose rate was calculated as 0.221 mSy^{-1} which was subtracted from the calculated annual effective indoor dose rate to get the excess annual effective dose rate as shown on Table 5.6. The scatter plot (Figure 5.8) indicates that both indoor and outdoor are within the recommended limit of 1 mSvy-^{1} (ICRP, 2005).

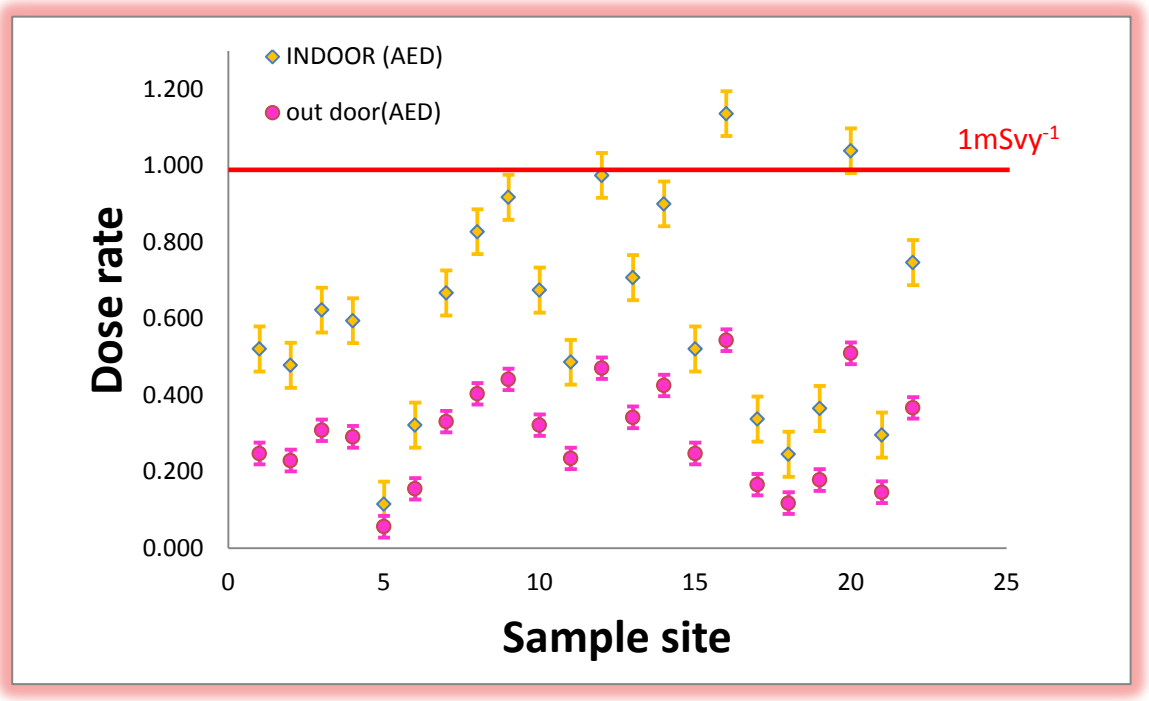

Figure 5.8: Comparison between indoor and outdoor annual effective dose rates obtained for the sand samples in this study. The recommended limit is 1$mSvy^{-1}$ (ICRP, 2005).

This value corresponds to the limit of radium equivalent which is 370 $Bqkg^{-1}$. Two samples exceeded the indoor annual effective dose rate recommended limit of 1 $mSvy^{-1}$, however none of the sample's excess indoor annual effective dose rate exceeded that limit. Table 5.7 shows absorbed dose rates and annual effective dose rate obtained in this study compared to the values obtained from construction sand in Kenya and around the world.

Table 5.7: Absorbed dose rates and annual effective dose rate in construction sands obtained in this study compared to that obtained in other parts of Kenya and the world.

Country	Outdoor Dose (nGy/h)	Indoor Dose (nGy/h)	Outdoor AED (mSv/y)	Indoor AED (mSv/y)	Reference
Kenya	121	167	0.30	0.61	This study
Kenya	-	152	-	0.74	Shikali, 2013, Kakamega
Saudi Arabia	114	212	0.14	1.04	Kinsara et al., 2014, Hail province.
Nigeria	-	73	-	0.36	Ayaji et al.,2013 Ogbomoso South-west Nigeria

CHAPTER SIX

CONCLUSION AND RECOMMENDATIONS

6.1 Conclusion

The activity levels of natural radionuclides of uranium, potassium and thorium in construction sand sampled from Tharaka region of Tharaka nithi County have been measured using NaI(Tl) gamma ray spectrometer. It is a region where all the remaining rocks from volcanicity are found hence it's suspected to have high radiation exposure levels. The radiological parameters associated with the construction sand have been determined hence the radiological effects on human beings due to the natural radionuclides from the sand.

The mean activity concentration of ^{40}K, ^{238}U and ^{232}Th in the samples was 1069 ± 46 $Bqkg^{-1}$, 96 ± 4 $Bqkg^{-1}$, and 53 ± 3 $Bqkg^{-1}$ respectively. The sand samples were collected from three main sub-counties within the county, Chuka- Igamba Ng'ombe, Tharaka north and Tharaka south. The mean activity concentrations of ^{40}K, ^{238}U and ^{232}Th in the samples were; 944 $Bqkg^{-1}$, 67 $Bqkg^{-1}$ and 54 $Bqkg^{-1}$ in Chuka- Igamba Ng'ombe. In Tharaka north the mean values of activity concentration recorded were 1413 $Bqkg^{-1}$, 42 $Bqkg^{-1}$, and 48 $Bqkg^{-1}$ for ^{40}K, ^{238}U and ^{232}Th respectively while in Tharaka south the computed values for ^{40}K, ^{238}U and ^{232}Th were 988 $Bqkg^{-1}$, 152 $Bqkg^{-1}$ and 45 $Bqkg^{-1}$ respectively.

Generally the average values of activity concentration of potassium were double the

world average value of 420 $Bqkg^{-1}$ (UNSCEAR 2008) in all the regions. This could be attributed to high silica content in the sand; since most of the rocks present are of volcanic origin, potassium is trapped in the silicate bond during cooling and solidification of igneous rocks. The samples from Tharaka south have an average activity concentration of uranium three times the value obtained in the other two regions. This could be due to the presence of high amounts of iron oxide in the region that help in absorbing of uranium from the circulating solutions.

The average calculated values of hazard indices; radium equivalent, external hazard and internal hazard were found to be 257 ± 13 $Bqkg^{-1}$, 0.69 ± 0.03 and 0.95 ±0.05 respectively. These values are below the acceptable limits of 370 $Bqkg^{-1}$ for radium equivalent and 1 for internal and external hazard indices (ICRP, 2005). This indicates that the construction sand from the region is fit to be used as building material and do not pose any risks to the inhabitants. However four samples taken from Tharaka south exceeded the recommended limit of 370 $Bqkg^{-1}$ especially the samples picked at the foot of Kijege and Ntugi hills due to high levels of uranium in the samples.

The average value of outdoor and indoor absorbed dose rates was 121 $nGyh^{-1}$ and 167 $nGyh^{-1}$ respectively. These values are above the world average of 54 $nGyh^{-1}$ and 84 $nGyh^{-1}$ (UNSEAR, 2008) for outdoor and indoor respectively. The average annual effective dose rate for outdoor and indoor gamma radiation from the samples was computed as 0.30 $mSvy^{-1}$ and 0.61 $mSvy^{-1}$ respectively. These values are above the world average of 0.07 $mSvy^{-1}$ and 0.41 $mSvy^{-1}$ respectively for outdoor and indoor

annual effective dose rate (UNSCEAR, 2008). None of the samples exceeded excess indoor annual effective dose rate and outdoor annual effective dose rate recommended dose constraint of 1 $mSvy^{-1}$ (ICRP, 2005). This indicates that the construction sand from Tharaka region of Tharaka Nithi County can be used for construction without any limitations because it does not pose any danger to the inhabitants in terms of acceptable limits.

6.2 Recommendations

Based on the results obtained, construction sand from this region is safe for construction purposes. However the sand mined at the foot of Kijege and Ntugi hills has elevated amounts of radionuclides concentration and particularly ^{238}U hence further studies need to be conducted around that region so that the policy makers can pass legislation on the safety of the sand to the general public. If the sand from these sites is used for building purposes, adequate ventilation in the room should be provided and the walls and floors well sealed to avoid risks of prolonged exposure to indoor radon. Furthermore the high levels of ^{238}U in soils reveals that the population is exposed to both indoor and outdoor radon.

This research has not exhausted analysis of other natural materials used for construction within the county. These include natural stones, clay fabricated bricks and red volcanic soils because most rocks and soils in the region are from volcanic origin hence need for a comprehensive analysis. Modeling and computational analysis of indoor radon concentration emanating from building materials to the rooms (buildings) based on the results of NORM is also essential. The study will help bridge the left gap.

REFERENCES

Abbady A. G. E. Uosif M. A. M. and El-Taher A. (2005). Natural radioactivity and dose assessment for phosphate rocks from Wadi El-mashal and El-Mahamid Mines in Egypt. *Journal of Environmental Radioactivity,* **84**: **65-78.**

Achola S. O. (2009). Radioactivity and elemental analysis of carbonatite rocks from parts of Gwasi area, south western Kenya. *M.sc Thesis (Physics)* University of Nairobi, Kenya.

Adel G. E. A and E-Taler, M. A. M. (2005). Natural Radioactivity and dose assessment for phosphate rocks from Wadi EL-Mashash and El-Mahamid mines in Egypt. *Journal of Radiation and Isotopes*. **84**: 65-78.

Adel G. E. A. (2004). Estimation of radiation hazard indices from sedimentary rocks in upper Egypt. *Applied Radiation and Isotopes,* **60**: 111-114.

Agora J. O. (2012). Assessment of Natural Radioactivity Levels and Radiation risk due to the Different Rock type in the Kerio Valley Region of Kenya. *M.sc Thesis (Physics).* Kenyatta University, Kenya.

Ajayi J.O., Paul J. and Bashiru B.B. (2013). Assessment of Radiological Hazard Indices of Building Materials in Ogbomoso, South-west Nigeria, *Environmental and Natural Resources Research* 3 (2): 128-132.

Atambo V. O. (2011). Determination of naturally occurring radioactive elements and radiation exposure levels in the soapstone quarries of Tabaka region of Kisii district, Kenya. *M.Sc Thesis (physics).* Jomo Kenyatta University of Agriculture and Technology, Kenya.

Bendibbie M. M., David M. M. and Jayanti P. P.(2013) Radiological analysis for suitability of Kitui south limestone for use as a building material. *International Journal of Fundamental Physical Sciences,* **3:**32-35.

Beretka J. and Matthew P.J. (1985). Natural radioactivity of Australian building materials, industrial wastes and by-products. *Health Physics,* **48**:87–95.

Cevic U. Damla N. Kobya A.I Celik N. Celik C. and Van A. (2009): Assessment of natural radioactivity of sand used in Turkey, *Journal of Radiation Protection,* 29: 61-74.

Chege W. M. (2007). Screening measurement of indoor radon-222 concentration by gamma ray spectrometry in Kenyatta University. *M.Sc Thesis (Physics)* Kenyatta University. Nairobi. Kenya.

Chege W. M. (2014). Modeling Radon and Thoron Exhalation and Measurements of Total Natural Radiation exposure in Mrima Hill, Kenya. *PHD Thesis (Physics)* Kenyatta University. Nairobi. Kenya.

Danilo C.V., Claubia P., Arno H. O., Talita O.S. and Zildete R. (2013) Modelling natural radioactivity in sand beaches in Guarapari, Brazil. *World Journal of Nuclear Science and Technology*, **3:** 65-71.

Debertin K. and Herlmer R. G. (1988). Gamma and X-Ray Spectrometry with Semiconductor Detectors. North Holland, Amsterdam.

European Commission (EC) 1998: Scientific seminar on radiation protection in relation to radon: Directorate General, Environment, Nuclear safety and Civil Protection.

European Commission (EC) (1999). *Radiation Protection 112—radiological protection principles concerning the natural radioactivity of building materials.* Directorate-General Environment, Nuclear Safety and Civil Protection.

Government of Kenya (GOK) (2011). Kenya national cancer control strategy 2011-2016. *Ministry of Public Health and Sanitation and Ministry of Medical Services Report*. Pg. 5-8.

Government of Kenya (GOK) (1985). Meru district environmental assessment report. *National Environment Secretariat, Ministry of Environment and Natural Resources.* Pg. 6-18.

Grupen C. (1996). Particle detectors, *Cambridge University Press*. pp **30-35.**

Gupta M., Chauhan R. P., Ajay G., Sushil K. and Sonkawade R.G.(2010). Estimation of radioactivity in some sand and soil samples. *Indian Journal of Pure and Applied Sciences*, **48:**482-485.

Hashim N. O., Rathore I. V. S., Kinyua, A. M. and Mustapha A.O. (2004). Natural and artificial radioactivity levels in sediments along the Kenyan coast. *Radiation Physics and Chemistry*, **71**: 805-806.

http://www.world-nuclear-news.org/ Naturally-occuring radioactive materials: Radiation and health effects Retrieved on 4/3/2015.

https://enwikibooks.org/wiki/Basic-Physics-of -Digital-Radiography: Basic physics of digital radiography. Retrieved on 3/8/2015.

http://www.tc3.edu/instruct/sbrown/stat/shape.htm. Measures of shapes : Kurtosis and Skewness. Retrieved on 16/8/2015.

International Atomic Energy Agency (1987): Preparation and certification of IAEA gamma spectrometry material. *Vienna RL/148.*

IAEA. (2005). Radiation Oncology Physics text book. A Handbook for teachers and students. IAEA. Vienna Austria.

IAEA (2009). International Atomic Energy Agency Annual Report, Vienna Austria.

International Commission on Radiological Protection (ICRP) 1993: Protection against Rn-222 at homes and at work. ICRP *publication 65:* Oxford; Pentagon press.

International Commission on Radiation Protection (ICRP), 2000. Protection of the public in situations of prolonged radiation exposure ICRP Publication 82; Ann. ICRP 29 (1–2), Pergamon Press, Oxford.

International Commission on Radiological Protection (ICRP), (2005). Low-dose Extrapolation of Radiation related cancer risks. ICRP Publication 99. Oxford: Pentagon press.

James E. P. (2014). Compton Scattering and Gamma Ray Spectrometry. *Department of Physics and Astronomy.* The University of Tennessee.

Kanoti J. R. (2001). The geology and mineralogy associated with mafic and ultramafic intrusives of the Mozambique belt in Mbeere and Tharaka Nithi Districts, eastern Kenya. *M. Sc thesis (geology),* University of Nairobi, Kenya.

Karama P.A. (2002). The high background radiation area in Ramsar, Iran: Geology, Norm Biology, LNT and possible regulatory fun. Proceedings of WM'02 conference, feb, 24-28, 2002, Tucson, AZ.

Kinyua R., Atambo V. O. and Ongeri R. M. (2011). Activity concentrations of ^{40}K, ^{232}Th and ^{228}Ra and radiation exposure of Tabaka soapstone quarries of the Kisii region, Kenya. *African Journal of Environmental Science and Technology*, **5**:682-688.

Kinsara A. A., Shabana E.I. and Qutub M.M.T. (2014). Natural Radioactivity in Some Building Materials Originating from a High Background Radiation Area. *International Journal for Innovation Education and Research*, 2 (6): 70-78.

Knoll, G. F. (1989). *Radiation Detection and Measurement* (Second edition) John Wiley and sons inc. New York USA, pp **214-216, 250**.

Knoll G.F. (1999). *Radiation Detection and Measurement* (Third edition) John Wiley & Sons, inc. New York USA, (Chapter 18-19).

Leo W. R. (1994). *Techniques for nuclear and particle physics experiments.* (Second edition). Springer verlag, Berlin. Pp **7-4, 177-197.**

Mangala J. M. (1987) A multi-channel X-ray fluorescence analysis of fluorspar ore and rock from Mrima hill, Kenya. *M.sc Thesis (Physics)* University of Nairobi, Kenya.

Merrie E. and Thomas G. (1997). Environmental radioactivity for natural and industrial and military sources, fourth edition. *Academic Press Elservier*, 162-210.

Mudd G. Gavin (2008): Radon sources and impacts: A review of mining and non-mining issues. *Journal of Environmental Scientific Biotechnology*, 7: 325-353.

Mustapha A. O. (1999). Assessment of human exposures to natural sources of radiation in Kenya. *Ph.D Thesis (Physics).* University of Nairobi. Kenya.

Mustapha A.O. Narayana D. G. Patel J. P. Otwoma D. (1997). Natural radioactivity in some building materials in Kenya and the contributions to the indoor external doses. *Journal of Radiation Protection Dosimetry,* 71(1): 65-69.

Mustapha A. O. Patel J. P. and Rathore I. V. S. (1999). Assessment of Human Exposures to Natural Sources of Radiation in Kenya. *Radiation Protection Dosimetry*, 82(4): 285-292.

Mutembei P.K. (2013). Concentration of iron in laterites from different localities of tunyai division in tharaka nithi county in kenya using magnetic separation. *M.SC Thesis (Chemistry)* Kenyatta University. Nairobi, Kenya.

Osoro M. K., Rathore I. V. S., Mangala M. J. and Mustapha A. O. (2011). Radioactivity in surface soils around the proposed sites for titanium mining in Kenya. *Journal of Environmental Protection*, **2**: 460-464.

Otwoma D., Patel J. P., Bartilol S., and Mustapha A. O. (2013). Estimation of annual effective dose and radiation hazard due to natural radionuclides in Mount Homa South-western Kenya. *Radation Protection Dosimetry.* pp 1-8.

Patel J. P. (1991). Environmental radiation survey of the area of high natural radioactivity of Mrima hill of Kenya. *Discovery and Innovation,* **3**: 31-35.

Schoeman J. J. (1951). A geological reconnaissance of the country between Embu and Meru. *Ministry of environment and natural resources, Mines and Geological Department.* Report number 17. Pp 9-28.

Shikali N. C. (2013). Radionuclide content of sands used for construction in Kakamega and associated indoor radium diffusion doses in *Kenyatta University. M.SC Thesis (physics)* Kenyatta University. Nairobi, Kenya.

Shikali C. Munji M. Ambusso W. (2014). Radionuclide content of sands used for construction in Kakamega County, Kenya and associated indoor radiation diffusion fluxes. *Journal of environmental and earth sciences,* 4 (15): 157-164.

Shoeib M. Y. and Thabayneh K. M. (2014). Assessment of natural radiation exposure and radon exhalation rate in various samples of Egyptian building materials. *Journal of Radiation Research and Applied Sciences,* 7(2): 174-181.

Sohrabi M. (1990). Recent radiological studies of high level natural radiation areas of Ramsar, Iran. International conference of high levels of natural radiation, Ramsar 3-7 Nov, 1990. IAEA, Vienna 71-86.

Sunta C. M. (1993). A review of studies of high background areas of s-w coast of India, Ramsar, 3-7 Nov 1990, IAEA Vienna 71-86.

Turhan S., Baycan U.N. and Sen K. (2008). Measurement of Natural Radioactivity in building materials used in Ankara and assessment of external dose. *Journal of Radiological Protection,* **28:** 83-91.

United Nations Committee on Effects of Atomic Radiation, (1993). Exposure from natural sources of radiation. United Nations, New York.

United Nations Committee on Effects of Atomic Radiation, (1996). Exposure from natural sources of radiation. United Nations, New York. Annex A and B.

United Nations Scientific Committee on Effects of Atomic Radiation. (2000). Sources and effects of ionizing radiation. United Nations, New York. Annex A and B.

United Nations Scientific Committee on Effects of Atomic Radiation. (2008). Sources and effects of ionizing radiation. United Nations, New York. Vol 1.

Viega R. N., Sanchesa R. M., Anjosa K., Macarioa J., Iguatemya J. G., Aguiarb A. M. A., Santos B., Mosqueraa C., Carvalhoa M. and Baptista N. K. (2006). *Measurements of Natural Radioactivity in Brazilian Beaches sand. Radiation Measurements*, 346-369.

Wei, L., Zha, Y., Tao, Z., Hew, Chend and Yuan (1993). Epidemiological investigation in high background radiation areas in Yangjiang, China. p. 523-547 in: Proceedings of the International Conference on High Levels of Natural Radiation, Ramsar, 1990. IAEA, Vienna, 1993.

World health organization (WHO) (2002), National cancer control programs, Policies and managerial guidelines, 2nd edition.

Xinwei L. and Xiaolan Z. (2008): Radionuclide content and associated radiation hazards of building materials and by products in Baoji, West China. *Journal of Radiation Protection Dosimetry*, 128: 471-476.

APPENDIX 1

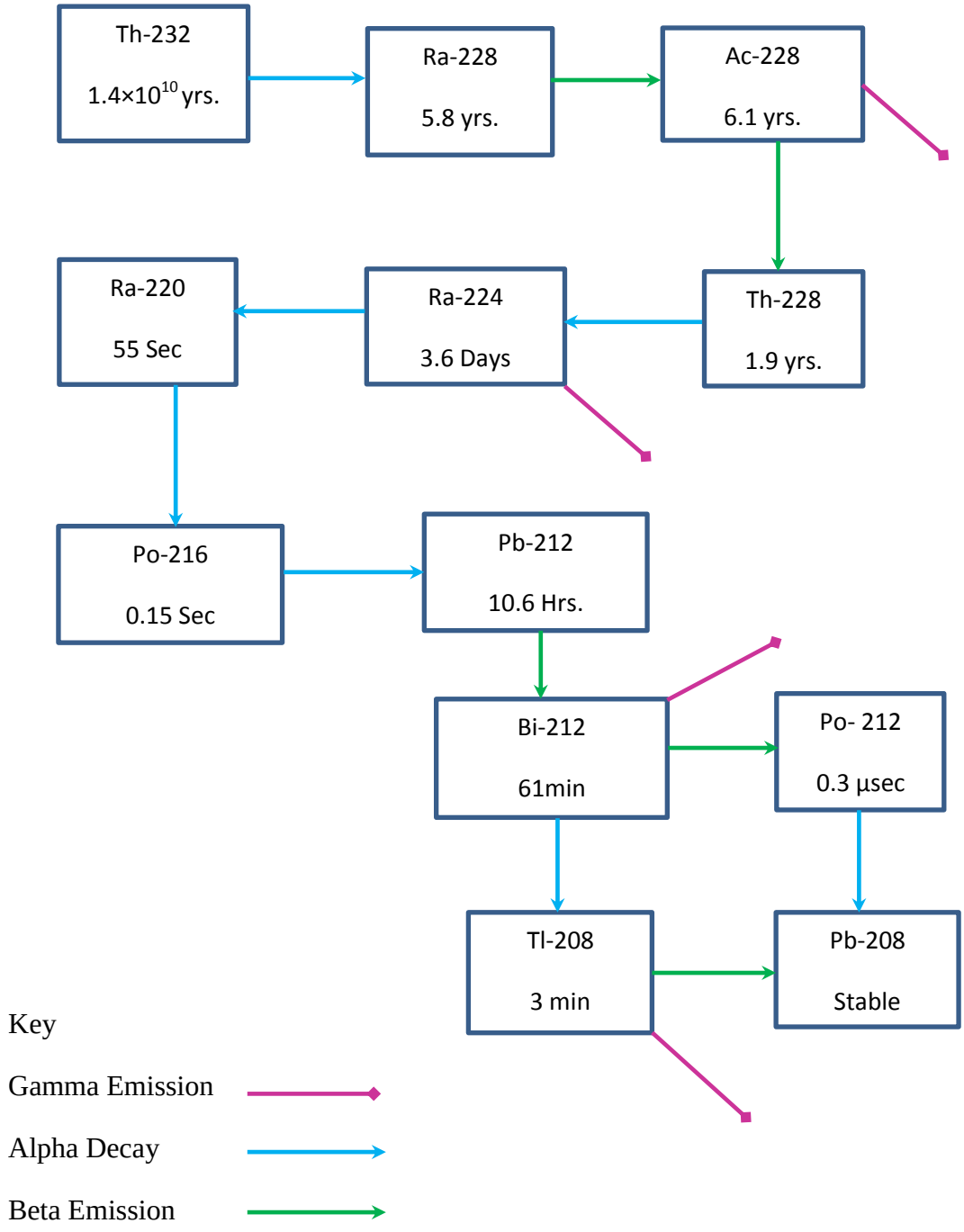

Figure A1: Radioactive Decay in Thorium Series (http://www.world-nuclear-news.org, 2014).

APPENDIX 2

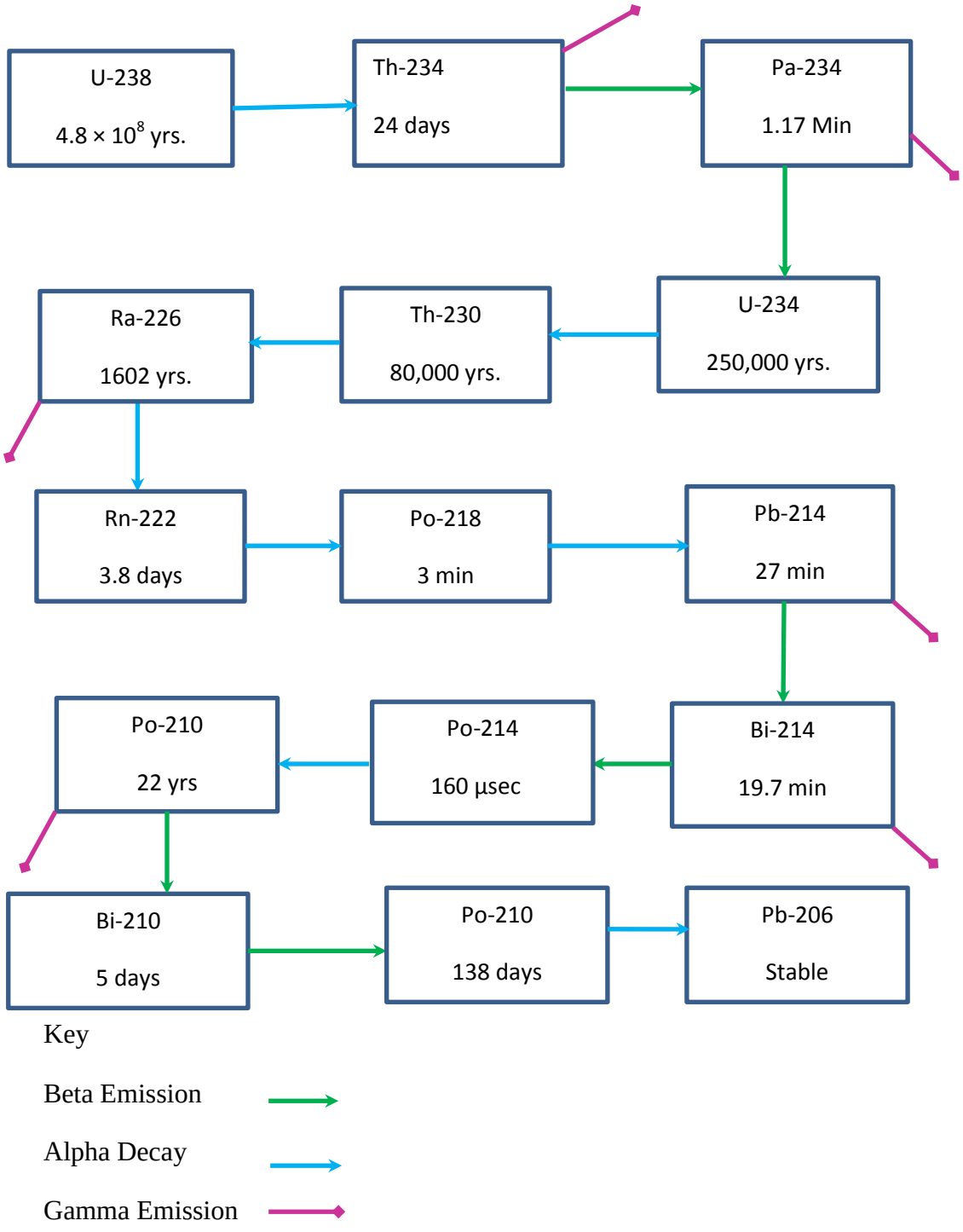

Figure A2: Radioactive decay in Uranium series (http://www.world-nuclear-news.org, 2014).

APPENDIX 3

Figure A3 (a): Kijege hills in Tharaka south (Taken on 29/11/2014).

Figure A3 (b)*:* Gulley carrying sand from the withered rocks in the hills (Taken on 29/11/2014).

Figure A3 (c): Sand mined in river Ruguti (Taken on 28/11/2014).

Figure A3 (d): Equipment used in the field. The Geiger Muller counter was used for in situ measurements of radioactivity levels while the GPS was used to locate the sample collection site (Taken on 30/11/2014).

APPENDIX 4

Figure A4 (a): Gneiss rock with high quartz content from Tharaka south (Taken on 29/11/2014).

Figure A4 (b): Sedimentary rock of granitic origin with high quartz content from Tharaka north (Taken on 30/11/2014).

APPENDIX 5

Figure A5 (a): Yellowish brown sand sample from Tharaka-south (Taken on 29/11/2014).

Figure A5 (b): Reddish brown sand sample from Igamba-Ng'ombe (Taken on 28/11/2014).

Figure A5 (c): Grayish brown sand sample form Tharaka south (Taken on 29/11/2014).

Figure A5 (d): Dark brown sand sample from Tharaka north (Taken on 30/11/2014).